ApJ in press
Preprint typeset using LaTeX style emulateapj v. 9/08/03

THE GEMINI DEEP DEEP SURVEY. VII. THE REDSHIFT EVOLUTION OF THE MASS-METALLICITY RELATION[1,2]

S. Savaglio[3], K. Glazebrook[3], D. Le Borgne[4], S. Juneau[5,6], R. G. Abraham[4], H.-W. Chen[7,11], D. Crampton[6], P. J. McCarthy[8], R. G. Carlberg[4], R. O. Marzke[9], K. Roth[10], I. Jørgensen[10], R. Murowinski[6]

ApJ in press

ABSTRACT

We have investigated the mass-metallicity (M-Z) relation using galaxies at $0.4 < z < 1.0$ from the Gemini Deep Deep Survey (GDDS) and Canada-France Redshift Survey (CFRS). Deep K and z' band photometry allowed us to measure stellar masses for 69 galaxies. From a subsample of 56 galaxies, for which metallicity of the interstellar medium is also measured, we identified a strong correlation between mass and metallicity, for the first time in the distant Universe. This was possible because of the larger base line spanned by the sample in terms of metallicity (a factor of 7) and mass (a factor of 400) than in previous works. This correlation is much stronger and tighter than the luminosity-metallicity, confirming that stellar mass is a more meaningful physical parameter than luminosity. We find clear evidence for temporal evolution in the M-Z relation in the sense that at a given mass, a galaxy at $z \sim 0.7$ tends to have lower metallicity than a local galaxy of similar mass. We use the $z \sim 0.1$ Sloan Digital Sky Survey M-Z relation, and a small sample of $z \sim 2.3$ Lyman break galaxies with known mass and metallicity, to propose an empirical redshift-dependent M-Z relation, according to which the stellar mass and metallicity in small galaxies evolve for a longer time than in massive galaxies. This relation predicts that the generally metal poor damped Lyman-α galaxies have stellar masses of the order of $10^{8.8}$ $M_\odot$ (with a dispersion of 0.7 dex) all the way from $z \sim 0.2$ to $z \sim 4$. The observed redshift evolution of the M-Z relation can be reproduced remarkably well by a simple closed-box model where the key assumption is an e-folding time for star formation which is higher or, in other words, a period of star formation that lasts longer in less massive galaxies than in more massive galaxies. Such a picture supports the downsizing scenario for galaxy formation.

Subject headings: galaxies: fundamental parameters – galaxies: abundances – galaxies: ISM – ISM: H II regions – galaxies: evolution – cosmology: observations

1. INTRODUCTION

Our exploration of the evolution of the cosmic metal enrichment relies mainly on two methods. One is based on the detection of absorption lines in the neutral interstellar medium (ISM) of galaxies crossing QSO sight-lines (Prochaska et al. 2003), and gives information of one line of sight in the galaxy. The other uses emission lines of the warm ISM (HII regions) detected in the integrated galaxy spectra, and is observationally much more challenging at high redshift because important lines get very weak and redshifted to the near IR.[12]

The warm ISM metallicity and the mass of galaxies are strongly correlated in the low-z Universe (Lequeux et al. 1979). More massive galaxies have higher metallicity than less massive galaxies. This mass-metallicity (M-Z) relation has never been detected at high redshift. In fact, measurements of the stellar mass (strongly correlated with the dynamical mass; Brinchmann & Ellis 2000) require deep optical/NIR photometry of faint targets, and are not easy to obtain for a sufficiently large sample for which metallicity is known.

To explore any evolution with redshift, luminosity, as a proxy for mass, can be used instead, although luminosity is more difficult to interpret physically than mass. The metallicity of large $0.3 < z < 1$ galaxy samples has been studied in relation to the galaxy luminosity by Kobulnicky et al. (2003), Lilly, Carollo, & Stockton (2003), Kobulnicky & Kewley (2004) and Liang et al. (2004). Kobulnicky & Kewley (2004; hereafter KK04) have used about 200 galaxies from the Team Keck Redshift Survey (TKRS; Wirth et al. 2004) and found a luminosity-metallicity (L-Z) relation displaced towards higher luminosities with respect to the same relation detected at $z = 0$ (Kennicutt 1992; Jansen et al. 2000). This suggests a redshift evolution of the L-Z relation. At higher z, only a handful of galaxies have been studied so far

[1] Based on observations obtained at the Gemini Observatory
[2] Based on observations obtained at the Canada-France-Hawaii Telescope
[3] Department of Physics & Astronomy, Johns Hopkins University, Baltimore, MD 21218, [kgb; savaglio]@pha.jhu.edu
[4] Department of Astronomy & Astrophysics, University of Toronto, Toronto ON, M5S 3H8 Canada, [leborgne; abraham; carlberg]@astro.utoronto.ca
[5] Département de physique, Université de Montréal, 29 00, Bld. Édouard-Montpetit, Montréal, QC, Canada H3T 1J4, sjuneau@astro.umontreal.ca
[6] NRC Herzberg Institute for Astrophysics, 5071 W. Saanich Rd., Victoria, BC, Canada, [david.crampton; murowinski]@nrc-cnrc.gc.ca
[7] Center for Space Sciences, Massachusetts Institute of Technology, 70 Vassar St., Bld. 37, Cambridge, MA 02139, hchen@space.mit.edu
[8] Carnegie Observatories, 813 Santa Barbara St, Pasadena, CA 91101, pmc2@ociw.edu
[9] Department of Physics and Astronomy, San Francisco State University, San Francisco, CA 94132, marzke@stars.sfsu.edu
[10] Gemini Observatory, 670 North A'ohoku Place, Hilo, HI 97620, [jorgensen; kroth]@gemini.edu
[11] Hubble Fellow

[12] Stellar features can also be used as metallicity estimator, however this way it is much harder to obtain accurate information for a single galaxy (Pettini et al. 2000; de Mello et al. 2004).

(Pettini et al. 2001; Shapley et al. 2004) and again low metallicities are found compared to galaxies with similar luminosity at low redshifts.

Do we also expect the M-Z relation to evolve with time? Shifts of the L-Z relation will arise from simple luminosity evolution (i.e. changing the mass–to-light ratio) and this is well documented in galaxies over $0 < z < 1$ (Schade et al. 1996; Vogt et al. 1996). In particular passive fading of stellar populations (as observed in early-type galaxies, e.g. Aragon-Salamanca et al. 1993) would shift L-Z but not M-Z. However, astrophysically, we would expect the star-formation activity over $0 < z < 1$ to manifest itself in changes of metallicity as well as mass. The question is what is the form of this change and can it be detected?

From a different prospective, the cold ISM, damped Lyman-α (DLA) galaxies detected in QSO spectra have metallicities $\sim 1/10$ solar at $z \sim 0.7$ (Prochaska et al. 2003), i.e. one order of magnitudes lower than line emitters at similar redshifts (KK04). Part of the discrepancy could be due to the fact that the absorption lines statistically probe the outskirt of galaxies, where metallicity is lower, while emission line flux originates in the central more metal rich region (Chen, Kennicutt, & Rauch 2005; Ellison et al. 2005; Schulte-Ladbeck et al. 2005). Another possibility is that DLAs and line emitters are probing different galaxies all together. Unfortunately, so far no information on masses of DLA galaxies is available.

In this work we present the first attempt to derive the mass-metallicity relation in high redshift galaxies selected by near-IR photometry down to small masses. The sample is selected from the $0.4 < z < 1$ galaxies of the Gemini Deep Deep Survey (GDDS; Abraham et al. 2004) and Canada-France Redshift Survey (CFRS; Crampton et al. 1995; Le Fèvre et al. 1995; Lilly et al. 1995). Masses were estimated using deep optical-NIR photometry and metallicities using optical spectroscopy. For consistency with GDDS, metallicities for the CFRS galaxies were recomputed using emission line fluxes published by Lilly et al. (2003; hereafter LCS).

Before continuing our discussion it is important to emphasize that measurements of physical parameters can differ by some factor, depending on how they are estimated. For instance, masses can change by a factor of ~ 2, depending on which initial mass function (IMF) is applied. Similarly, metallicities can be different by a factor of $2-3$, depending on which set of lines and/or calibrator are considered (Kennicutt, Bresolin & Garnett 2003; KK04). Thus, we paid special attention to deriving results, and comparing them with other works, in a consistent fashion.

The paper is organized as follows: in §2, we describe the sample section from the GDDS; in §3 we present the GDDS composite spectrum used to derive an overall stellar absorption and dust extinction; §4 & §5 describe the stellar mass and the metallicity derivations, respectively, for the GDDS and the CFRS samples; §6 & §7 are about the luminosity-metallicity and mass-metallicity relations, respectively; in §8 we discuss possible systematic effects; §9 is on the modeling of the redshift evolution of the M-Z relation; the discussion and the concluding remarks are in §10 and §11. Throughout the paper we adopt a $h \equiv H_o/100 = 0.7$, $\Omega_M = 0.3$, $\Omega_\Lambda = 0.7$ cosmology (Spergel et al. 2003).

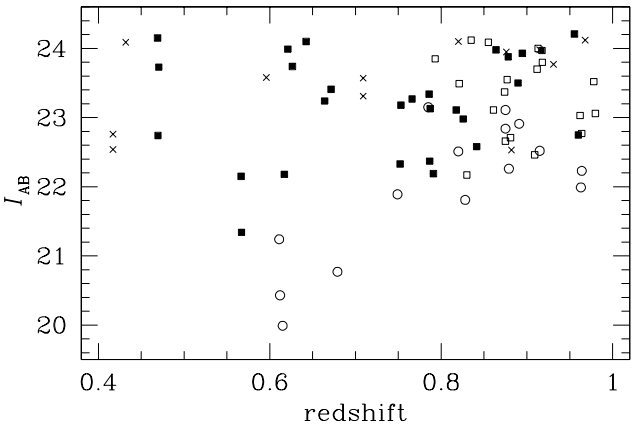

FIG. 1.— The I_{AB} magnitude vs. redshift of the GDDS galaxies at $0.40 < z < 0.98$. The selected galaxies are shown as filled squares; 25% and 75% are classified as late-type and intermediate-type galaxies, respectively. For the rest of the sample, pure early-type and intermediate-type galaxies are shown as empty circles and squares, respectively. The non-selected intermediate-type galaxies, generally show only [OII] emission and no other line. One galaxy (SA22-2107) is not included in the selected sample because it is contaminated by an interloper. Crosses are galaxies not included in the sample because one or more emission lines are corrupted or outside the spectral range.

2. THE GDDS SAMPLE SELECTION

The Gemini Deep Deep Survey[13](Abraham et al. 2004) is the deepest survey targeting galaxies in the redshift desert ($0.8 < z < 2$). It is based on spectra obtained with the Gemini Multi Object Spectrograph (GMOS), operating in nod & shuffle mode (Glazebrook & Bland-Hawthorn 2001; Cuillandre et al. 1994) for precise sky subtraction. The survey has been primarily targeting galaxies with photometric redshifts $z > 0.8$ and $K < 20.6$, but other objects were included to fill gaps in the GMOS masks. The galaxy sample is complete down to K (Vega) magnitudes $K = 20.6$, and I magnitudes $I_{AB} = 24.7$. For comparison, the I_{AB} magnitude limit for the TKRS of KK04 and CFRS of LCS is $I_{AB} \approx 24$ and 22.5, respectively. For the $z < 1$ galaxies, GDDS is much deeper than CFRS because it was designed to reach $L^\star$ for local galaxies to $z = 2$, the same flux limit is sub-$L^\star$ at $z < 1$. The observed GDDS I magnitude corresponds to the rest-frame B magnitude for a galaxy at $z \sim 0.7$.

In terms of stellar mass the GDDS is complete (for $z < 2$) down to $M_\star = 10^{10.8}$ M$_\odot$ for all galaxies (Glazebrook et al. 2004). The completeness increases to $M_\star = 10^{10.1}$ M$_\odot$ and $10^{9.6}$ M$_\odot$, for star-forming galaxies at $z < 2$ and $z < 1$, respectively. More than 300 spectra were taken, of which about 200 are $z > 0.3$ galaxies with secure redshifts. The slit aperture used for the observations was 0.75×1.1 arcsec^2, and the signal in the direction perpendicular to the dispersion was extracted over ~ 0.8 arcsec. The wavelength range observed is typically 5500–9800 Å.

For this work, the GDDS sample selection is based on the requirement that the spectrum of the galaxies

[13] For the Public Data Release, visit http://www.ociw.edu/lcirs/gdds.html

(with secure redshift) covers the spectral interval of the [OII]λ3727, [OIII]$\lambda\lambda$4959, 5007 and Hβ lines. These are the lines necessary to determine the metallicity using the R_{23} calibrator (Pagel et al. 1979). The redshift range is thus restricted to $0.40 < z < 0.98$. Figure 1 shows I_{AB} vs. z for GDDS galaxies in this redshift interval (73). Twelve of these are excluded from the sample because one or more lines are corrupted or just outside the spectral range (which to some extend depends also on the position of the slit in the mask); one object is clearly contaminated by an AGN and another by an interloper, so are excluded from the sample. Among the 59 remaining objects, the selected 28 (filled squares) show [OII], Hβ and [OIII] emission; 25% and 75% are classified as late type and intermediate type, respectively. The other non-selected galaxies are early type (empty circles) or intermediate type (empty squares) with only weak or no [OII] emission, and no other emission line.

Our detection limit for emission line fluxes is a function of redshift (the spectral sensitivity is higher in the blue than in the red) and is well represented in the observed redshift interval by the function

$$f_{lim}(10^{-18}\ \mathrm{ergs}^{-1}\ \mathrm{cm}^{-2}) = 4.31z - 1.12 \qquad (1)$$

We detected line fluxes down to $(0.6-3.2)\times10^{-18}$ erg s^{-1} cm^{-2} in the interval $z = 0.4-1$ (3σ). For 4 galaxies, the [OIII] or Hβ emission is below detectability, so a limit was derived for the metallicity. The CFRS detection limit of LCS is $\sim 2\times10^{-17}$ erg s^{-1} cm^{-2}, i.e. a factor of $6-30$ higher than our flux limit.[14]

Spectra of the selected sample are shown in Figures 2–5. For 15 of the galaxies we also obtained *Hubble Space Telescope* (HST) *Advances Camera for Survey* (ACS) images (Figure 6). For the majority of them a disk structure is apparent. To measure fluxes, the continuum was estimated from the mean value in two small spectral regions before and after the line. Errors are derived using the noise spectrum, and generally agree (within a factor of 1.5) with the pixel-to-pixel standard deviation in the signal spectra. For about 1/3 of the galaxies, the Hγ line is also detected. All line fluxes, not corrected for slit aperture losses, are reported in Table 1. The spectra of SA22-2541 and SA15-4662 show spurious lines due to order overlap in the GMOS mask (see Abraham et al. 2004). Order overlap has negligible effect on the emission flux, therefore metallicity, measurements.

The multi-band photometry for the GDDS is provided by the Las Campanas Infrared Survey (LCIRS; McCarthy et al. 2001; Chen et al. 2002) and is generally accurate (errors are generally less than 1/10 mag; Abraham et al. 2004). K and z' band magnitudes (Table 1) are key parameters used to measure the stellar mass (Glazebrook et al. 2004). The rest-frame B-band absolute magnitude is derived by approximating the SED between the V, R and I bands with a power law.

3. THE GDDS COMPOSITE SPECTRUM

We created a composite spectrum from all galaxies in the GDDS sample, for two reasons. One is to estimate the stellar absorption used to correct the Balmer emission lines; the other is to estimate an average value of dust extinction, via the Balmer decrement. Fluxes of Balmer emission lines in Table 1 are only corrected for the stellar Balmer absorption, and not for the dust extinction.

3.1. *Stellar Balmer absorption*

To combine all spectra together, each spectrum has been normalized to unity, by dividing the flux by its mean value in the interval $\lambda\lambda = 4200-4400$ Å. Thus each galaxy has the same weight in the composite spectrum (Figure 7). The best fit to the stellar continuum, obtained using Bruzual & Charlot (2003) stellar population synthesis models, is for a 50 Myr old stellar population and a visual extinction[15] for the stellar continuum $A^{\star}_V = 1.6$. A Calzetti extinction law (Calzetti 2001) and a solar metallicity are assumed. The model gives an acceptable fit when the dust extinction and the age of the stellar population span $0.7 < A^{\star}_V < 2.0$ and $30-200$ Myr, respectively. If the dust extinction is in the higher or lower end, only ages below 80 Myr or in the range $100-200$ Myr are acceptable, respectively. In these intervals, the emission fluxes in the composite generally vary by less than 5%. The best-fit model is only used for the Balmer absorption correction and does not give a comprehensive description of the underlying stellar population. In general, the properties (e.g., dust extinction, metallicity and ages) of the stellar component in the optical (dominated by small and intermediate mass stars) can differ from those of the young star-forming component represented by the optical emission lines. Moreover, strictly speaking, the true $A^{\star}_V$ is very likely lower than the estimated value, because of blue-flux spectral loss due to the atmospheric dispersion. This has little effect on the Balmer absorption features.

From the composite we derive an equivalent width EW correction for Hβ and Hγ absorptions of the order of 3.6 Å and 3.4 Å, respectively, depending on the underlying emission line FWHM. Changing the Hβ absorption EW by $\pm$%50 changes the metallicity by less than 0.1 dex in 83% of the galaxies, and on average by 0.06 dex. For the CFRS sample, LCS have used a Balmer absorption correction of 3 Å, with 2 Å uncertainty, as derived for local irregulars and spirals by Kobulnicky, Kennicutt, & Pizagno (1999). In extragalactic HII regions the correction is lower, with a typical EW of 2 Å (McCall, Rybski, & Shields 1985).

After subtracting the stellar continuum (bottom panel of Figure 7), emission line fluxes in the composite are measured and reported (relative to Hβ) in Table 2. Errors are estimated by using the standard deviation in the subtracted spectrum around each emission line.

3.2. *Balmer decrement and dust extinction correction*

The comparison between the Balmer decrement (high order Balmer emission line fluxes relative to the Hβ flux, after stellar absorption correction) observed in the composite spectrum and the theoretical value (in the case of no extinction, from atomic physics) provides a reasonable estimate of the mean dust extinction. The theoretical line ratios (Osterbrock, 1989) are only a weak

[14] The flux limit for TKRS is not available, because spectra are not flux calibrated.

[15] Throughout the paper $A^{\star}_V$ is the visual extinction of the stellar continuum, and A_V is the visual extinction affecting the Balmer emission lines.

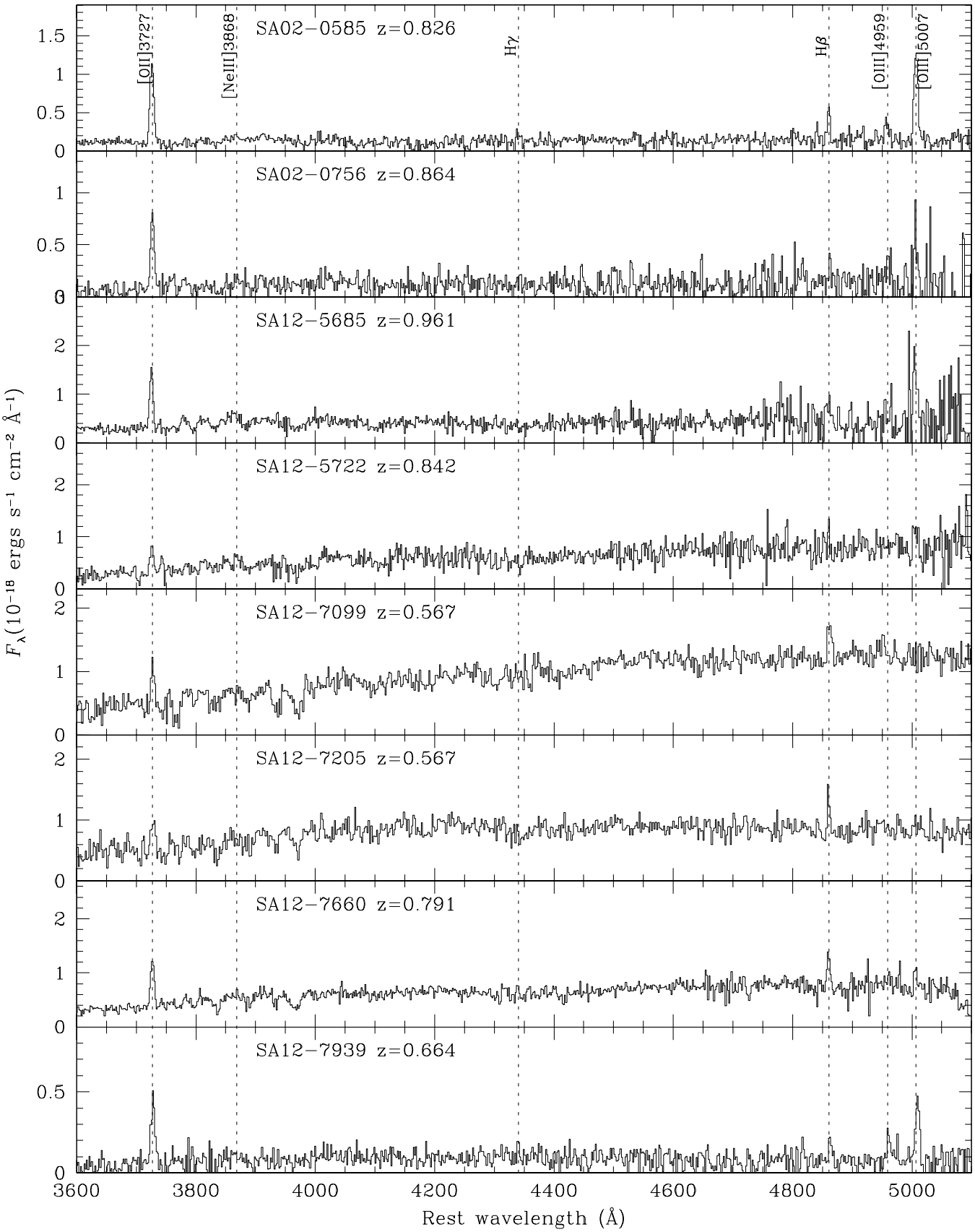

FIG. 2.— The sample of GDDS galaxies at $0.4 < z < 1$. Relevant emission lines are marked by the vertical dashed lines.

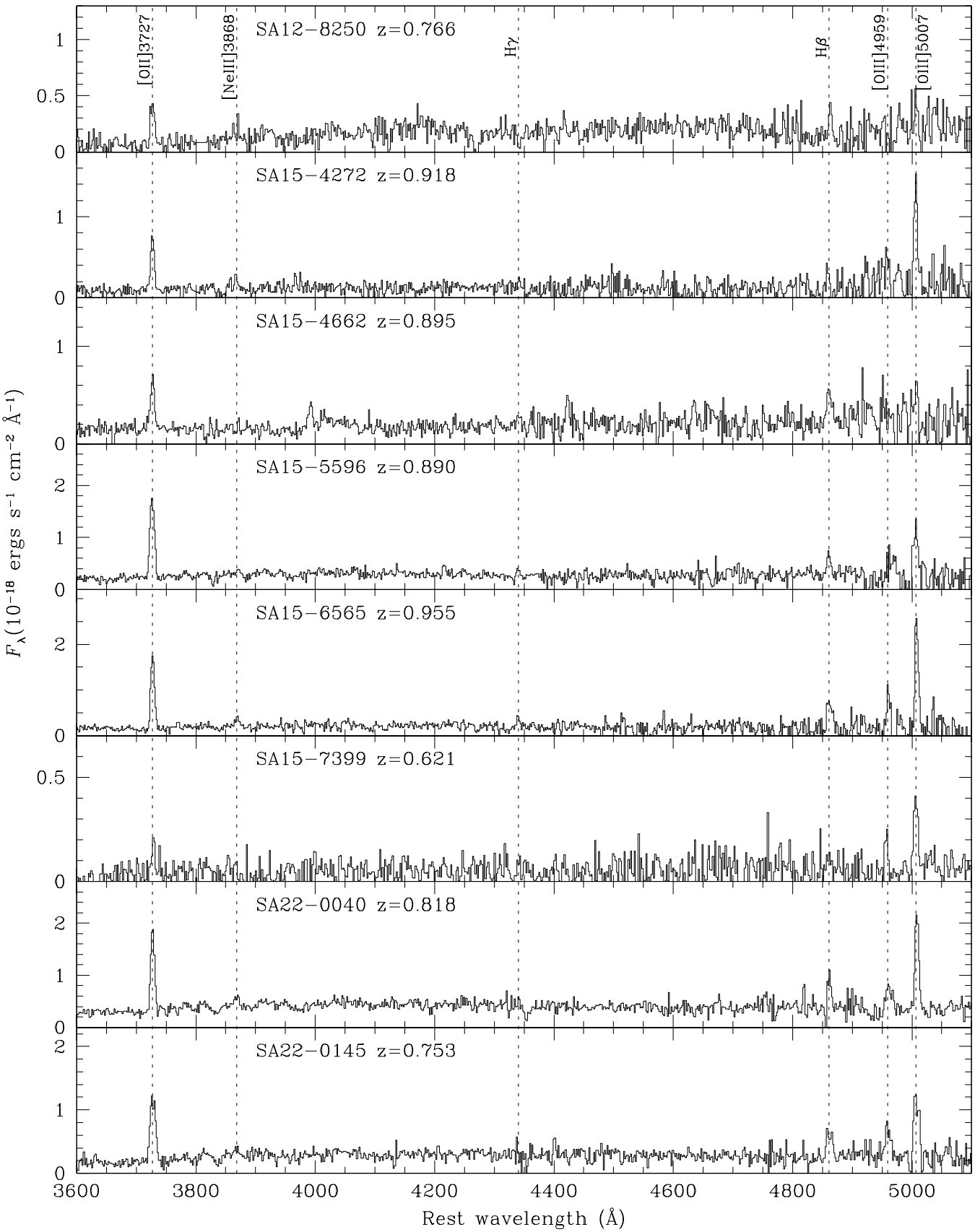

FIG. 3.— As in Figure 2. The spurious emission line at $\lambda \sim 4000$ Å in the spectrum of SA15-4662 is due to order overlap in the GMOS mask (see text).

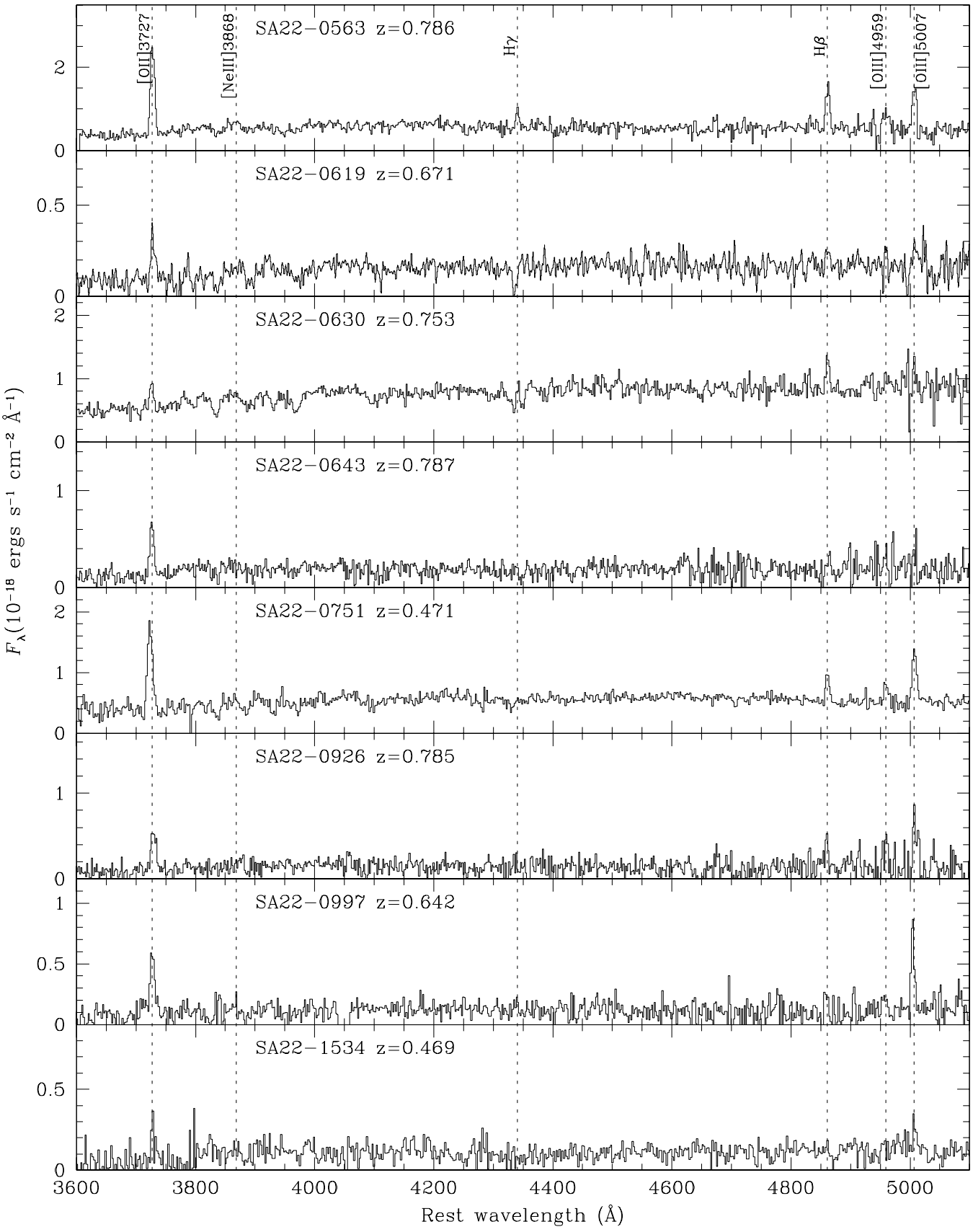

FIG. 4.— As in Figure 2.

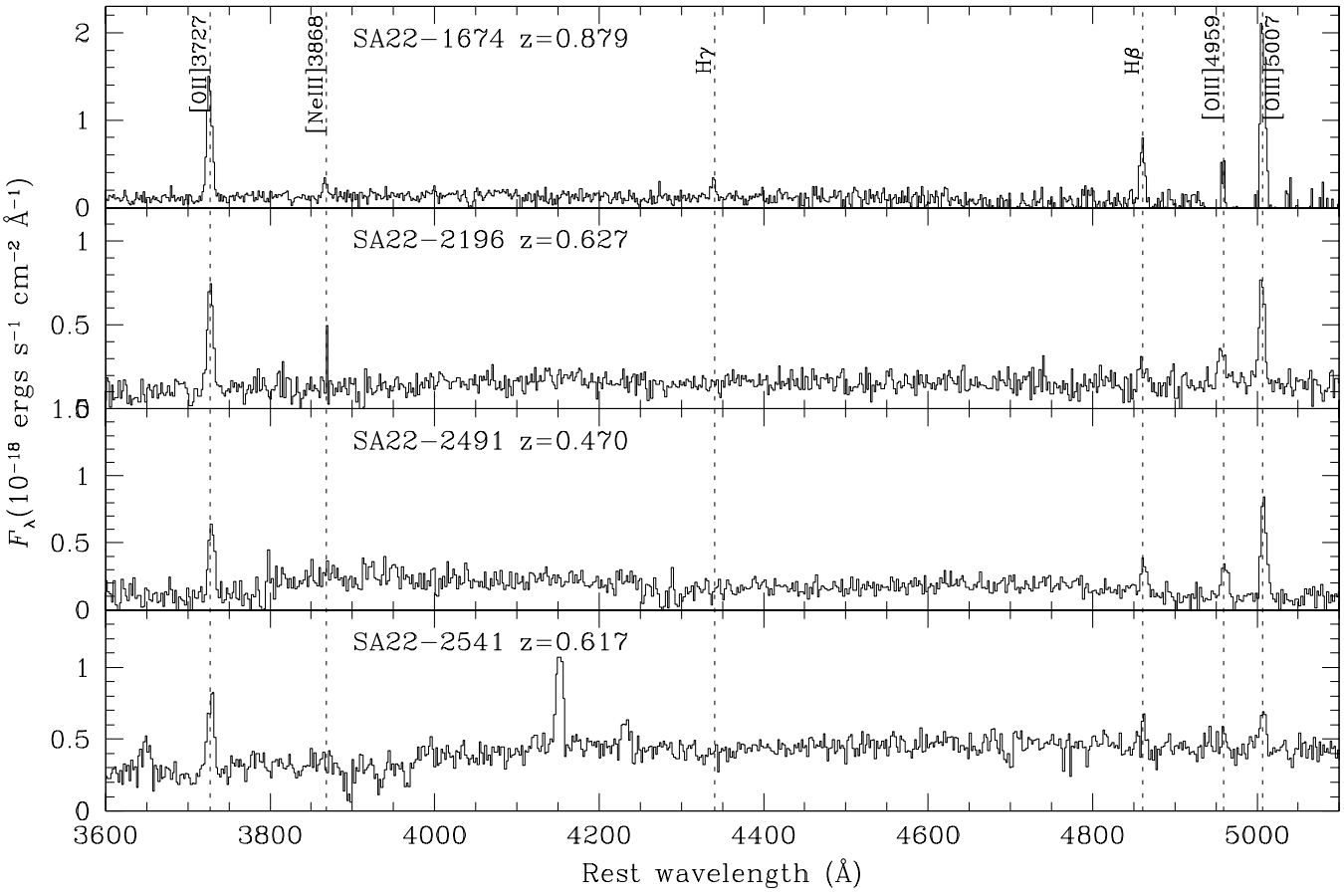

FIG. 5.— As in Figure 2. The two spurious emission lines at $\lambda \sim 4200$ Å in the spectrum of SA22-2541 are due to order overlap in the GMOS mask (see text).

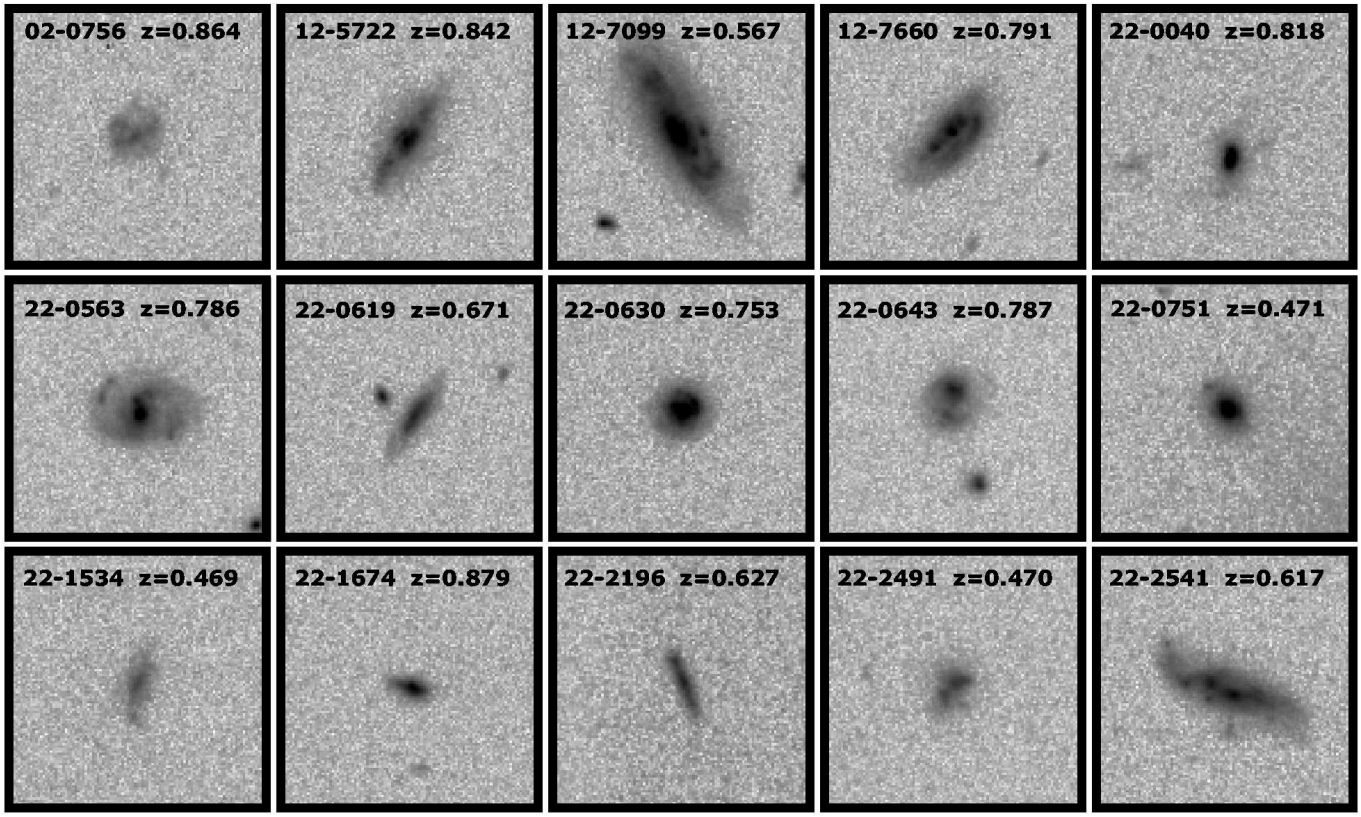

FIG. 6.— HST/ACS F814W images of 15 of the 28 GDDS selected galaxies. The size of the images is 5×5 arcsec^2.

function of the gas temperature, and are shown in Table 2 for $T = 10,000\ K$ and $5000\ K$. The visual extinction is estimated assuming the MW extinction law (practically unchanged for LMC or SMC extinctions). The error-weighted mean, from Hγ/Hβ through H8/Hβ, is $A_V = 2.13 \pm 0.32$ or 1.92 ± 0.32 for $T = 10,000\ K$ or $5000\ K$, respectively.

In principle the assumed visual extinction can be checked by comparing line EW ratios (almost unaffected by dust) with the extinction-corrected flux ratios. This method is not very accurate because it is based on the assumption that the continuum flux ratio at the [OII] and Hβ wavelengths is nearly one (Kobulnicky & Phillips 2003). Nonetheless, in the subsample of 15 galaxies for which an accurate estimate of the emission line EWs is possible, we found a good match between EW ratios and flux ratios for $A_V \sim 2$.

We compare our A_V with other estimates derived for different samples. Cid Fernandes et al. (2005) found an empirical relation between the visual gas extinction A_V and the visual stellar extinction $A_V^\star$ using data from the Sloan Digital Sky Survey (SDSS). If transformed to take into account a small difference in the extinction law adopted by us, this relation is:

$$A_V = 3.173 + 1.841 A_V^\star - 6.418\ \log\left(\frac{\mathrm{H}\alpha}{\mathrm{H}\beta}\right)_{th} \qquad (2)$$

where $(\mathrm{H}\alpha/\mathrm{H}\beta)_{\mathrm{th}}$ is the line flux ratio expected from atomic physics theory. Considering that from the composite spectrum best fit we derived an upper limit for the stellar extinction of $A_V^\star = 1.6$, then $A_V < 3.2$ or < 3.0, for $T = 10,000\ K$ or $5000\ K$, respectively. We also consider that Eq. 2 is based on data at $z \sim 0.1$ and can vary in the high-z Universe.

An extinction for the ISM similar to ours ($A_V = 2.4 \pm 0.4$) was derived from the Hα/Hβ value (after stellar absorption correction) measured in the SDSS composite spectrum, the "cosmic optical spectrum" (Glazebrook et al. 2003). LCS assumed $A_V = 1$, and this could be more appropriate for relatively brighter (hence likely less extincted) galaxies as in the CFRS sample. This gives Hγ/Hβ = 0.39, which is significantly larger than our Hγ/H$\beta = 0.29 \pm 0.02$ (Table 2). An older and more extincted stellar population model (older than 100 Myr, and $A_V^\star > 1.5$) would give a higher Hγ/Hβ in our composite, then a lower A_V. However, the fit is much worse, the χ^2 is 3 times higher.

Calzetti (1997) found a mean visual extinction in a sample of 19 starburst galaxies of $A_V = 1.35$ with a 1σ dispersion of 0.77 magnitudes. The higher value in our sample can be an indication of a higher dust content in galaxies that are generally more massive and more metal rich than the local starbursts (Brinchmann et al. 2004).

The Hγ emission line is detected in 10 GDDS galaxies (Table 1), so the Balmer decrement provides the dust extinction in these spectra individually. For this subsample we found $< A_V >= 1.66$ with a dispersion of 1.3 magnitudes, indicating that galaxies for which Hγ is detected tend to be less extincted. However, because the errors are always higher than 0.5 mag, we ignore A_V estimated this way. It is worth noticing that the median stellar mass

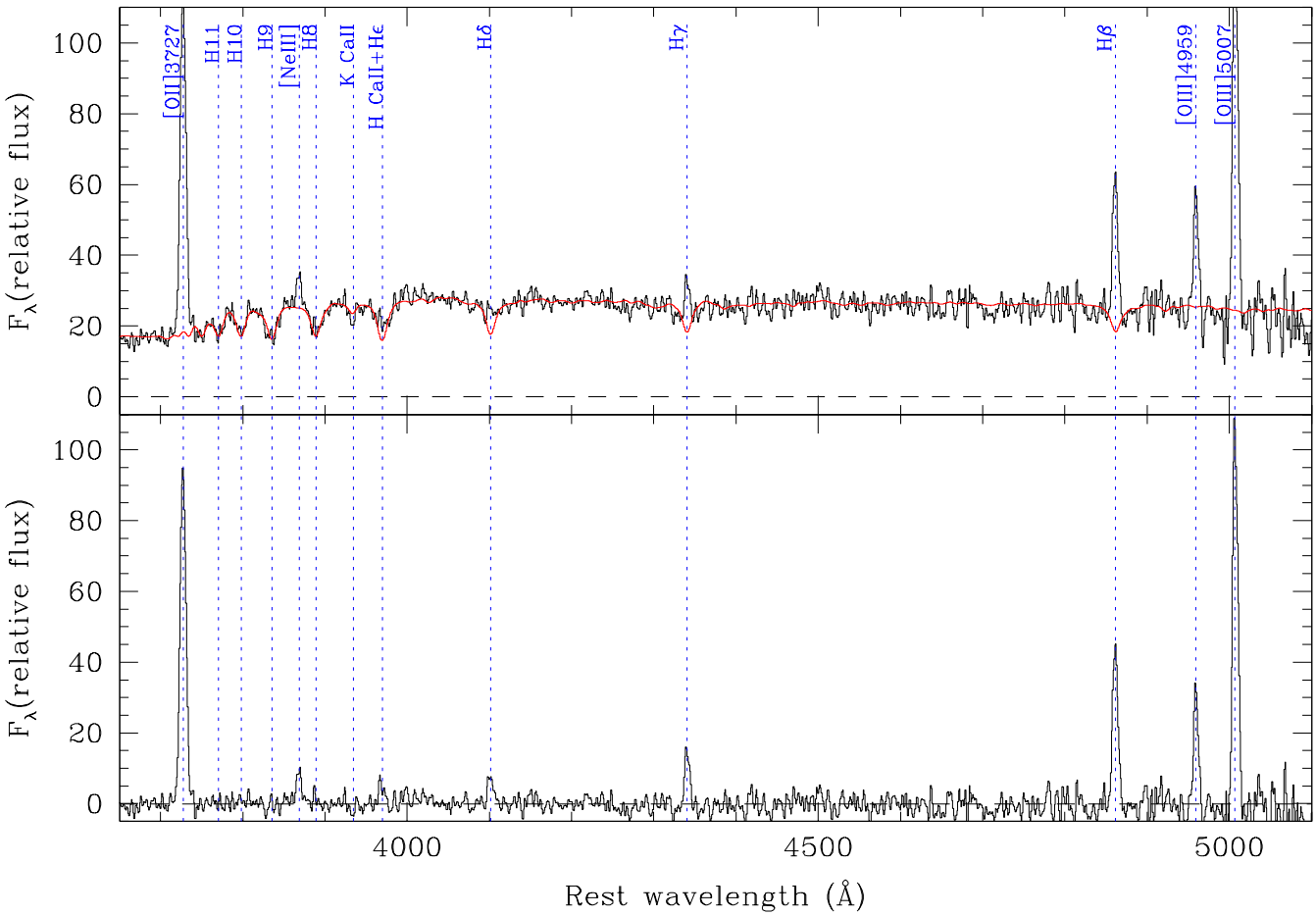

FIG. 7.— Composite spectrum of 26 $0.4 < z < 1$ GDDS galaxies. The dotted vertical lines mark the relevant features. The smooth spectrum in the upper panel is the "best-fit" model (Bruzual & Charlot 2003) of the stellar component, obtained for a 50 Myr old stellar population and a visual extinction $A_V^\star = 1.6$ (metallicity is assumed to be solar). The lower panel shows the emission lines after the stellar continuum subtraction. Fluxes measured from the composite spectrum are listed in Table 2. The Balmer stellar absorption profile has been subtracted from each galaxy spectrum before measuring emission line fluxes, and is of the order of 3.6 and 3.4 Å (equivalent width) for Hβ and Hγ, respectively, depending on the emission line FWHM.

for these galaxies ($M_\star = 10^{9.4}$ M$_\odot$) is lower, but close, to the median value for the whole sample ($M_\star = 10^{9.6}$ M$_\odot$), suggesting that if the dust extinction were larger for more massive galaxies, this effect is not apparent in our intermediate redshift sample.

The visual extinction uncertainty (0.3 mag) does not affect very much the metallicity estimates from line ratios because the wavelength baseline of the emission lines used (from [OII] to [OIII]) is not very large ($3727 - 5007$ Å). Consequentially our results are relatively unaffected for small variations of A_V. We will adopt $A_V = 2.1 \pm 0.3$ and discuss results for $A_V = 1$. In the GDDS sample the metallicity decreases on average by 0.2 dex if A_V goes from 0 to 3.

4. STELLAR MASSES

The stellar mass of galaxies in the GDDS and CFRS samples have been estimated using the procedure described in Glazebrook et al. (2004) and also used in Juneau et al. (2005). The galaxy SED is modeled using the multi-band photometry. Galaxy model spectra are provided by PÉGASE.2 (Fioc & Rocca-Volmerange 1997, 1999). The fitted parameters are the stellar dust extinction (in the range $0 < A_V < 2$), the age of the stellar population, and the metallicity. The star formation rate is assumed to decline exponentially, with e-folding time ranging from $\tau = 0.1$ to 500 Gyr, combined with a bursty component with $\tau = 100$ Myr and variable mass fraction. The best-fit SED gives a M/L_K, from which masses are reliably derived. The IMF used is that derived by Baldry & Glazebrook (2003; hereafter BG03), and gives a total stellar mass 1.8 or 1.2 times smaller than for a Salpeter or a Kroupa IMF, respectively. The difference with Salpeter IMF is mainly in the low mass stars. The error in the stellar masses includes uncertainties on A_V, τ and mass fraction of the burst. Our mass estimates, based on the rest-frame optical-NIR photometry, is much more robust than when based on rest-frame UV light, which is strongly affected by very uncertain parameters like dust extinction and recent star formation. This SED-fitting method gives a mass accuracy generally better than a factor of two for the $z > 0.8$ GDDS galaxies (Glazebrook et al. 2004). A similar method was recently tested against other stellar mass estimates, and was found to be generally robust and accurate (Drory, Bender & Hopp 2005).

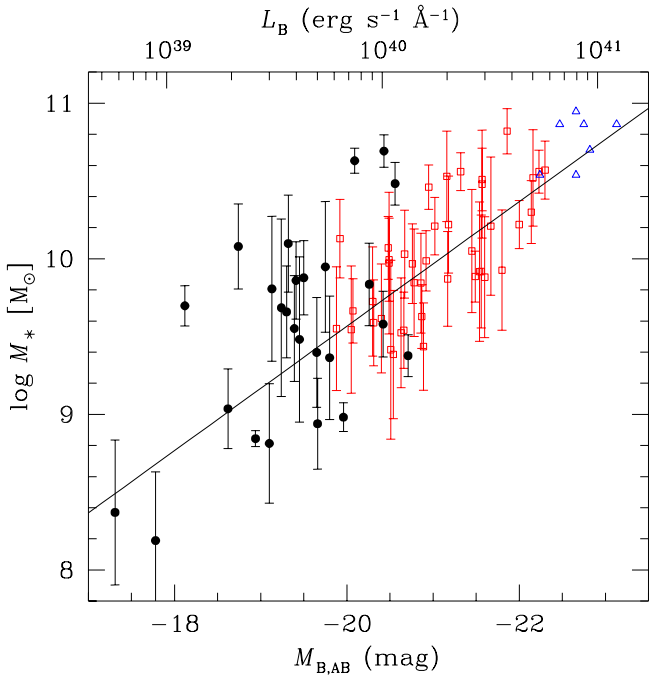

FIG. 8.— Stellar Mass and B absolute magnitude (or luminosity, upper horizontal axis) for the GDDS (filled circles) and CFRS (empty squares) $z < 1$ galaxies. The open triangles are the $z \sim 2.3$ LBGs (Shapley et al. 2004) after correcting the stellar mass for BG03 IMF. The straight line marks a constant ratio of stellar mass to B luminosity, in solar units, of $M_{\star,\odot}/L_{B,\odot} = 0.3$.

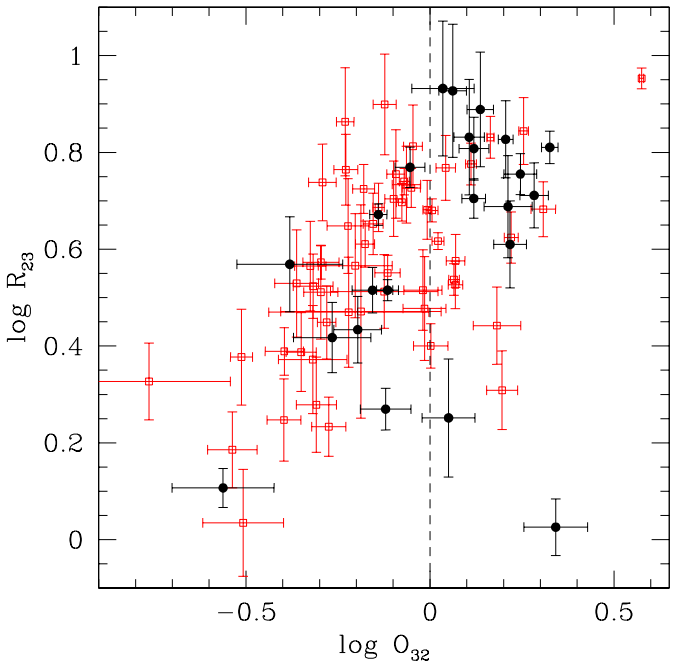

FIG. 9.— R_{23} vs. O_{32} for the GDDS (*filled circles*) and the CFRS (*open squares*) galaxies. The dust correction is not applied. The CFRS points are calculated using emission line fluxes from LCS. The dashed line marks the region with $O_{32} = 1$. The large fraction of galaxies with $O_{32} > 1$ in GDDS with respect to CFRS is an indication of lower metallicity, and/or higher dust extinction, and/or higher ionization. The O_{32} value decreases by 0.4 dex if the dust correction goes from $A_V = 0$ to 3.

For the GDDS galaxies in our $z < 1$ sample, the $VIz'K$ photometry allowed reliable mass estimates to be derived for 27 galaxies, out of 28 (Table 1). For one galaxy, the stellar mass could not be calculated for incomplete photometric information. The median error is 0.3 dex, and the errors are lower than a factor of two and three for 55% and 94% of the objects, respectively. For many galaxies, only upper limits to the K magnitude are available, therefore stellar masses rely on the z' magnitude. These masses were not derived in Glazebrook et al. (2004), but their uncertainties are still acceptable, as the observed z' band corresponds to the rest-frame V band at redshift ~ 0.7. These errors are typically ~ 0.15 dex higher than those for galaxies with measured K magnitude. In three cases for which neither K nor z' are available, mass errors are larger.

The sample median redshift and redshift interval are $z = 0.79$ and $0.47 < z < 0.96$, respectively. The lowest and the highest masses are $M_\star = 10^{8.2}$ M$_\odot$ and $10^{10.7}$ M$_\odot$, and the sample is complete down to $M_\star = 10^{9.6}$ M$_\odot$.

For the CFRS sample of 69 galaxies, VIK photometry is used and masses are measured for 42 galaxies (Table 3). The mass error is always smaller than 0.6 dex (less than a factor of 4), and the median error is 0.3 dex. The lowest measured mass is $M_\star = 10^{9.4}$ M$_\odot$, i.e. 16 times higher than the lowest stellar mass in the GDDS. The highest mass is $10^{10.8}$ M$_\odot$. The median redshift and interval are $z = 0.68$ and $0.479 < z < 0.915$, respectively.

The total number of galaxies for which we measured masses is 69. For 56 of these we also determined metallicities (see §5).

Figure 8 shows the stellar mass and the B absolute magnitude (or luminosity) for the GDDS and CFRS samples. It is apparent that GDDS galaxies are less massive (on average 2.24 times) and fainter (~ 1.75 magnitudes, or a factor of 5 in flux) than CFRS galaxies. GDDS galaxies are on average > 1.1 mag fainter in K than CFRS galaxies. The fact that the ratio between the mean CFRS B luminosity and the mean GDDS B luminosity is larger than the mass ratio, indicates that GDDS galaxies are on average more dust extincted than CFRS galaxies.

As a reference, the LBGs at $z \sim 2.3$ (Shapley et al. 2004, also in Figure 8) are much brighter and more massive than the CFRS galaxies. (LBG masses are scaled to take into account the different IMF used, and the recycling into the ISM, which Shapley et al. did not include and which makes the final stellar masses 1.4 times smaller.)

5. THE METALLICITY USING THE R$_{23}$ PARAMETER

Emission line fluxes of [OII]λ3727, Hβ, and [OIII]$\lambda\lambda$4959, 5007 provide an estimate of metallicity[16] through the R_{23} calibrator. When the [OIII]λ4959 emission line is barely detected, the flux is assumed from atomic physics to be 0.34 times the [OIII]λ5007 flux, and the error propagated accordingly. The R_{23} parameter, as defined by Pagel et al. (1979), is

$$\log R_{23} = \log\left(\frac{f_{[\mathrm{OII}]\lambda3727} + f_{[\mathrm{OIII}]\lambda\lambda4959,5007}}{f_{\mathrm{H}\beta}}\right) \equiv x \quad (3)$$

[16] We express metallicity in terms of the number of oxygen atoms relative to hydrogen: $12 + \log(\mathrm{O/H})$.

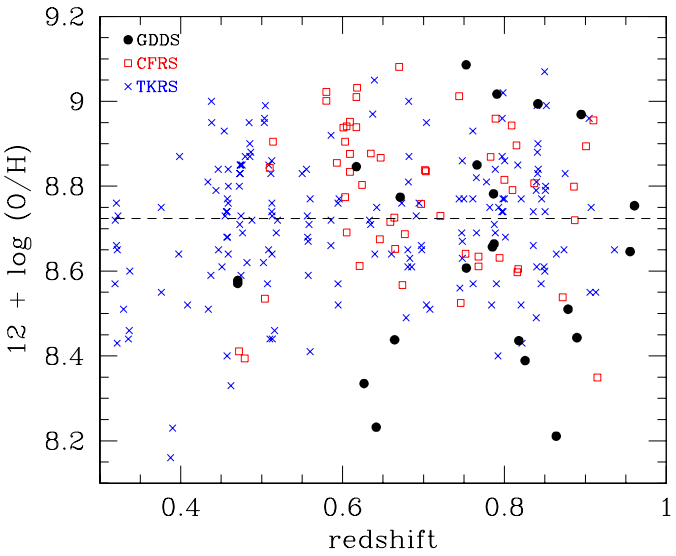

FIG. 10.— Metallicity as a function of redshift for GDDS (filled circles), CFRS (empty squares) and TKRS (crosses, from KK04). The mean metallicities in the GDDS, CFRS and TKRS are $12 + \log(\mathrm{O/H}) = 8.63 \pm 0.26$, 8.78 ± 0.17 and 8.72 ± 0.17, respectively. The mean total metallicity (dashed line) is $12 + \log(\mathrm{O/H}) = 8.72 \pm 0.17$, i.e. roughly solar. We do not detect any significant redshift evolution for the total sample of 261 galaxies, from $z = 0.32$ to $z = 0.96$ (time interval of 4.3 Gyr).

We also define the O_{32} parameter:

$$\log O_{32} = \log \left(\frac{f_{[\mathrm{OIII}]\lambda\lambda 4959,5007}}{f_{[\mathrm{OII}]\lambda 3727}} \right) \equiv y \qquad (4)$$

used to correct for the ionization. The R_{23} and O_{32} for GDDS galaxies are reported in Table 1 and are corrected for dust extinction. When dust extinction is applied, R_{23} increases and O_{32} decreases. O_{32} decreases by 0.4 dex if one corrects for A_V in the range $0 - 3$.

The ionization-sensitive O_{32} not corrected for dust in GDDS and CFRS (Figure 9) is > 1 in 62% & 27% of the galaxies, respectively. In the ~ 200 TKRS galaxies, KK04 found that 32% have $O_{32} > 1$. However, because KK04 used equivalent widths (not very sensitive to dust extinction) this fraction would be higher if unextincted fluxes are used instead. As noted by Kewley & Dopita (2002), O_{32} is higher not only in highly ionized or dusty regions, but also in low metallicity regions. In fact, in high metallicity regions, most of the nebular cooling occurs through far-IR oxygen lines, so the [OIII] emission becomes weak and the $O32$ parameter decreases.

The generally higher O_{32} in the GDDS with respect to CFRS (Figure 9) suggests that GDDS galaxies are more ionized and/or more extincted and/or less metal rich than CFRS galaxies. Additional evidence for more extinction in GDDS was provided in § 4.

The LBGs studied by Pettini et al. (2001) all have $O_{32} > 1$ and $R_{23} > 5$. The difference between these and our $z \sim 0.7$ galaxies likely implies lower metallicities for LBGs, not surprising at higher redshifts.

5.1. *The GDDS and CFRS metallicity*

The average metallicity of galaxies can be derived through different calibrators which use R_{23} and O_{32}. Initially proposed by Pagel et al. (1979), the R_{23}-metallicity relation was reformulated by several authors with the aid of the ionization-sensitive parameter O_{32} (Edmunds & Pagel 1984; Dopita & Evans 1986; McGaugh 1991; Pilyugin 2001; Kewley & Dopita 2002; KK04). The difference between the different calibrators can be as high as 0.2 dex, with the theoretical methods giving generally higher metallicities than the empirical methods (KK04). Another limit of the R_{23} calibrator is its double solution. In fact, at low metallicity, when the electron temperature T_e is high enough to keep the gas collisionally ionized, R_{23} scales with metallicity. But when the metallicity reaches a limit, the gas cooling occurs through the far-IR oxygen lines, then the R_{23}-metallicity dependence turns around, i.e. R_{23} decreases for higher metallicity. This happens when R_{23} is of the order of 10 and $12 + \log(\mathrm{O/H}) \sim 8.3$. In the turnover region, the metallicity is easily $0.2 - 0.4$ dex more uncertain because the two solutions are close and both possible. To break the degeneracy, other methods requiring other lines can be used, for instance [NII] and [SIII] (Denicoló, Terlevich, & Terlevich 2002; Pettini & Pagel 2004; Bresolin et al. 2005). However, at high redshift this requires expensive NIR spectroscopy, not easily accessible. Because T_e is sensitive to metallicity, the [OIII]λ4363/[OIII]λ5007 temperature-sensitive ratio gives the most reliable method (Kobulnicky et al. 1999). However [OIII]λ4363 is a weak line, useful only when the spectral S/N is high.

When the only available set of lines is [OII], [OIII] and Hβ, as in our and all cases where optical spectroscopy is available for high-z galaxies, the mass and the age of the galaxy can be used to break the degeneracy, as massive and evolved galaxies are typically metal rich. As the galaxies in our sample are generally massive, and our R_{23} is generally far from the turnover region, we will only consider the upper branch solution. This is supported by results on galaxies with similar luminosities and redshifts in TKRS and CFRS, for which other metallicity diagnostics indicated that the upper branch solution was correct (KK04, LCS).

Among the different calibrators, the empirical one proposed by McGaugh (1991) is the most commonly adopted. KK04 compared some of them, discussed possible biases, and concluded that the best one is represented by a mean value between McGaugh's and the theoretical one given by Kewley & Dopita (2002). The new calibrator is approximated, for metallicities higher than $12 + \log(\mathrm{O/H}) = 8.4$, by the following expression:

$$12 + \log(\mathrm{O/H}) = 9.11 - 0.218x - 0.0587x^2 - 0.330x^3 - \\ +0.199x^4 - y(0.00235 - 0.1105x - 0.051x^2 - 0.04085x^3 - \\ +0.003585x^4) \qquad (5)$$

Roughly speaking, the metallicity of Eq. 5 is not too different from McGaugh's, on average 0.07 dex higher in the range $8.4 < 12 + \log(\mathrm{O/H}) < 9.3$.

For this work, we used Eq. 5. For 4 galaxies, R_{23} is in the turnover region, and the metallicity is more uncertain. In these cases (when $12 + \log(\mathrm{O/H}) < 8.4$) we used the McGaugh calibrator and applied the small positive correction of 0.07 dex (as derived from the comparison with KK04). These galaxies do not change much our findings on the M-Z distribution at $z \sim 0.7$ (see §7).

GDDS metallicities are reported in Table 1 (calculated for $A_V = 2.1 \pm 0.3$). The mean value (and 1σ dispersion) is $12 + \log(\mathrm{O/H}) = 8.63 \pm 0.25$. This is only about 0.07 dex higher for $A_V = 1$. Errors on metallicities include the emission flux and A_V uncertainties only. The mean error, is 0.12 dex. Systematic uncertainties are generally higher than the measured errors for large metallicities. For 4 galaxies with an upper limit on Hβ or [OIII] flux, a lower or upper limit on the metallicity are provided, respectively.

LCS used for the CFRS sample the calibrator provided by McGaugh (1991) and $A_V = 1$. For consistency with GDDS, we have re-calculated metallicities, applying Eq. 5 (Table 3). Errors in the metallicities include an arbitrary uncertainty on A_V of 0.3 mag. Also for this sample, galaxies with an upper limit on Hβ or [OIII] fluxes provide a lower or upper limit on the metallicity, respectively. Two galaxies with no line detection, have no information on the metallicity. Table 3 also lists old LCS metallicities for the upper branch. Our new mean metallicity and error are $12+\log(\mathrm{O/H}) = 8.78 \pm 0.17$ and 0.07 dex, respectively (the LCS mean is 0.05 dex lower).

Figure 10 shows $12 + \log(\mathrm{O/H})$ as a function of redshift, for the GDDS, CFRS and TKRS samples. The mean metallicity of all 261 galaxies is $12 + \log(\mathrm{O/H}) = 8.72 \pm 0.17$, i.e. roughly solar[17]. Although the redshift range ($0.3 < z < 1.0$) corresponds to a time interval of 4.3 Gyr, no redshift evolution is detected (i.e. no significant metallicity-redshift correlation). We emphasize that galaxies in this plot include all masses, therefore the presence of a mass-metallicity relation at these redshifts (see §7) may obscure any redshift evolution of metallicity.

6. LUMINOSITY-METALLICITY RELATION AT $Z \sim 0.7$

In Figure 11 we show metallicity vs. B absolute magnitude (or B luminosity) for the GDDS (filled circles), CFRS (open squares) and the TKRS (crosses; KK04) galaxies. The GDDS+CFRS sample (79 galaxies) shows a 4σ significant correlation. The linear bisector best fit (Feigelson & Babu 1992) is expressed by:

$$12+\log(\mathrm{O/H}) = (-0.280\pm0.045)M_{\mathrm{B,AB}}+(2.977\pm0.937) \quad (6)$$

The fit does not change much (although the significance is slightly lower) if $A_V = 1$ is assumed for the GDDS galaxies.

In Figure 11, we show this bisector fit (solid line) together with the one found by KK04 for 177 TKRS galaxies [$12 + \log(\mathrm{O/H}) = -0.193 M_{\mathrm{B,AB}} + 4.900$, long-dashed line]. The short-dashed line is the L-Z relation for the SDSS 53,000 $z \sim 0.1$ galaxies (Tremonti et al. 2004; hereafter T04), which is very similar to the one found by Jansen et al. (2000) for the local Nearby Field Galaxy Survey (NFGS).

KK04 note that galaxies in their sample have higher luminosities with respect to local galaxies with similar metallicities, suggesting a redshift evolution of the L-Z relation. This is confirmed by the GDDS+CFRS sample, but our low-luminosity galaxies seem to have lower metallicities than the TKRS galaxies. This can only in part be due to the slightly different mean redshifts (0.71

[17] We assumed as a solar metallicity the value provided by Allende Prieto et al. (2001), which is $12 + \log(\mathrm{O/H})_\odot = 8.69$.

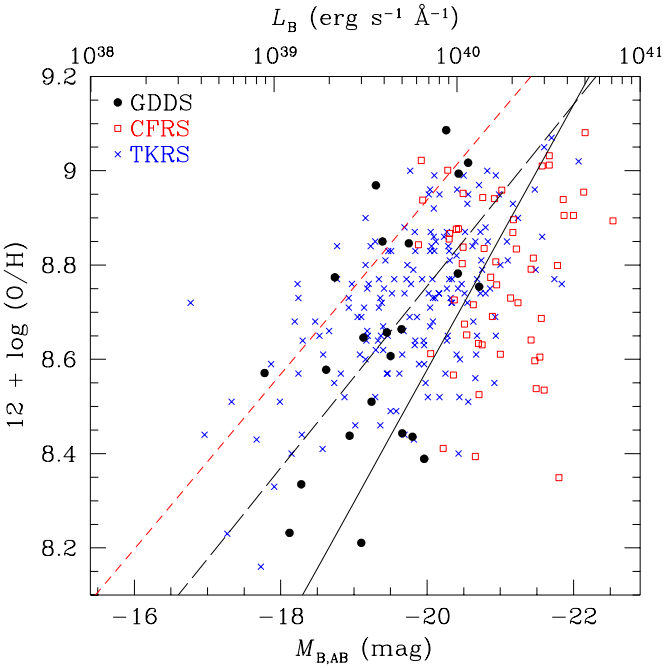

FIG. 11.— $12 + \log(\mathrm{O/H})$ as a function of B absolute magnitude $M_{B,AB}$ (or luminosity, upper horizontal axis) for the GDDS (filled circles), CFRS (open squares) and TKRS (crosses; KK04). The linear bisector fits (see text) for GDDS+CFRS and TKRS are shown as solid and long-dashed lines, respectively. The short-dashed line is the luminosity-metallicity relation found for the SDSS sample at $z \sim 0.1$ (Tremonti et al. 2004).

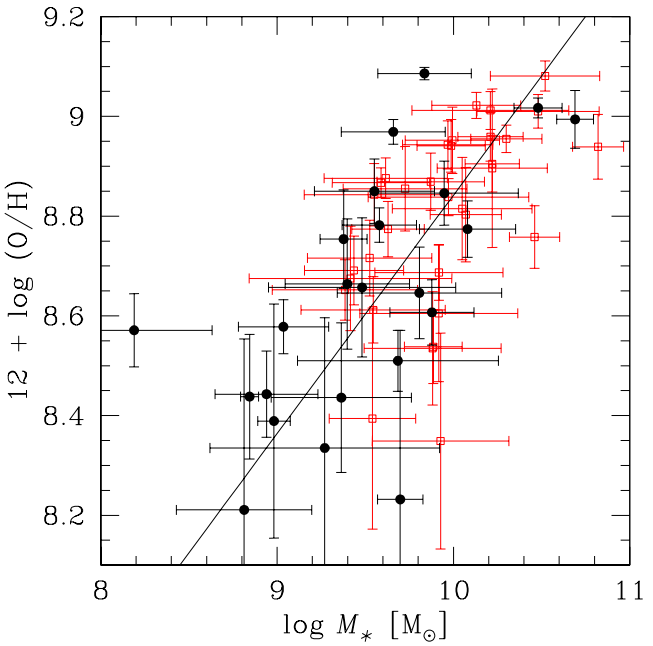

FIG. 12.— Metallicity as a function of stellar mass for GDDS (filled circles) and CFRS galaxies (open squares). Error bars include measurement errors but not possible systematic effects. The straight line is the linear bisector fit. The correlation is more than 6σ significant. The metallicity scale is as in Figure 11, and the mass scale spans three orders of magnitudes, as in the luminosity scale of the upper x-axis of Figure 11. This way it is possible to visually compare the point scatter in the two figures.

for GDDS+CFRS and 0.62 for TKRS) because the difference corresponds to only 0.5 Gyr. KK04 observe a steepening of the slope of the bisector fit from −0.16 to −0.24 (but this include the CFRS sample) going from $z \sim 0.3$ to $z \sim 0.9$. The difference might be related to the dust extinction correction, which can be a function of the stellar mass. While for the TKRS galaxies, EWs have been used which are almost insensitive to the dust correction, for our emission fluxes we have assumed a constant extinction correction both for GDDS and CFRS. If instead the dust correction is higher for more massive (than generally brighter) galaxies, the slope of the bisector fit would be lower. We also note that the large uncertainties and the different selection criteria for the three samples can explain the discrepancy.

7. MASS-METALLICITY RELATION AT $Z \sim 0.7$

Stellar masses and metallicities have been derived for a total of 57 GDDS and CFRS galaxies. One galaxy, SA15-4272, was removed from the GDDS sample for the large uncertainty on the Hβ flux. The median and mean redshift of the remaining 56 galaxies is $z = 0.69$ and 0.71, for GDDS and CFRS respectively. The stellar mass and metallicity distribution (Figure 12) are strongly correlated, at the level of 6.3σ. The linear bisector fit gives:

$$12+\log(\mathrm{O/H}) = (0.478\pm0.058)M_\star+(4.062\pm0.579) \quad (7)$$

The significance of the correlation is almost the same (6.6σ) if the 4 galaxies in the turnover region ($12 + \log(O/H) < 8.4$) are removed from the sample. The bisector slope becomes shallower, but consistent, with the slope for the whole sample (0.409 ± 0.050).

The scatter around the fit is ~ 0.2 dex. The scatter for the luminosity-metallicity distribution of Figure 11 is 65% higher. Results do not change much if $A_V = 1$ for the GDDS galaxies. The low-redshift half of the sample ($z < 0.7$) is not significantly differently distributed than the high-redshift half of the sample ($z > 0.7$).

We compare this distribution with the M-Z relation recently found by T04 for the $z = 0.1$ SDSS galaxies. To do that, we need to convert their relation to one consistent with our choice of IMF and metallicity calibrator.

T04 used the IMF provided by Kroupa (2001). The conversion from a Kroupa IMF to a BG03 IMF gives $M_{\star,\mathrm{BG03}} = M_{\star,\mathrm{K01}}/1.2$, or a difference of 0.08 dex.

T04 measured metallicities by modeling the emission lines and stellar continuum, using the approach described by Charlot et al. (in preparation), while for our sample we used the KK04 calibrator. A comparison between the two methods indicates that the T04 metallicities are at the most ~ 0.1 dex higher (this is mainly for the massive galaxies). The M-Z polynomial fit for the SDSS galaxies was recalculated using the KK04 calibrator (C. Tremonti, private communication).

The "converted" T04 M-Z relation (where the KK04 metallicity and BG03 IMF are used) is:

$$12+\log(\mathrm{O/H}) = -2.4412+2.1026\log M_\star-0.09649\log^2 M_\star \quad (8)$$

The overall difference with the T04 polynomial is not very large. The new relation and the $\pm1\sigma$ dispersion are shown in Figure 13.

In the same figure, we show our $z \sim 0.7$ galaxies (as in Figure 12, but error bars are omitted). The majority of the galaxies are distributed below the $z \sim 0.1$ relation, and preferentially these are galaxies with $M_\star < 10^{10}$ M$_\odot$, suggesting that massive galaxies reach high metallicities much earlier than low massive galaxies. In other words, the mass-metallicity relation evolves from being steep at high redshifts to being flatter at low redshifts. This picture of massive galaxies being more quiescent in recent times than less massive galaxies is also favored by recent results on the SFR density of the Universe calculated or measured for different galaxy stellar masses (Heavens et al. 2004; Juneau et al. 2005) according to which massive galaxies ceased forming stars (hence stopped enriching the ISM with metals) much earlier than low-mass galaxies. Low-mass galaxies have a long-lasting star-formation activity, and significantly produce stars and metals even in recent times. Those galaxies in the mass-metallicity diagram of Figure 13 will migrate with time from the left-bottom region to the middle region. A simple closed-box model which can explain this, is discussed in §9.2.

Our conclusion is not inconsistent with the relatively higher metallicities found for the generally massive LBGs (Shapley et al. 2004) and the star-forming galaxies at $z \sim 2$ of the K20 (de Mello et al. 2004). The rectangle in Figure 13 represents the region occupied by the LBGs. Masses have been converted to match our IMF and include recycling into the ISM (if recycling is ignored, stellar masses are 1.4 times higher). Metallicities are also converted to match our metallicity calibrator. Shapley et al. (2004) used the N2 calibrator (Pettini & Pagel 2004), which gives, for those stellar masses, metallicities ~ 1.4 to 2.3 times smaller, from the less massive to the most massive galaxy, than the KK04 calibrator (C. Tremonti, private communication). On average the difference is $\Delta[12 + \log(\mathrm{O/H})] = -0.23$.

8. POSSIBLE SYSTEMATIC EFFECTS

One of the puzzling results of the M-Z relation obtained for the star-forming galaxies by T04 and here, is that these galaxies appear to be generally metal rich for their stellar mass. For instance, the stellar mass of the Milky Way is $\sim 5 \times 10^{10}$ M$_\odot$ (Portinari et al. 2004). If its metallicity is approximately solar, $12 + \log(\mathrm{O/H}) \sim 8.7$, this is 0.4 dex lower than that predicted by the M-Z relation of the SDSS ($12 + \log(\mathrm{O/H}) \sim 9.1$).

First we have to consider that there are systematic differences between different metallicity calibrators (see §8.2). Moreover, it is well known that the metallicity decreases with the distance from the galaxy center (Garnett et al. 1997). According to Rolleston et al. (2000), in the Milky Way the oxygen abundance[18] goes from $12 + \log(\mathrm{O/H}) = 9$ to 8.6, at 6 kpc and 12 kpc from the center, respectively, with a radial gradient of −0.067 dex kpc^{-1}. Although the quantitative result depends on the empirical method used to measure metallicity, and although some extragalactic studies indicate lower central metallicities (Kennicutt et al. 2003), it is likely that the metallicity is higher than the average if the slit aperture used to collect the galaxy signal is small. The fiber aperture for the SDSS sample ($3''$) corresponds to a me-

[18] This is derived using absorption lines in the photosphere of B-type dwarf stars.

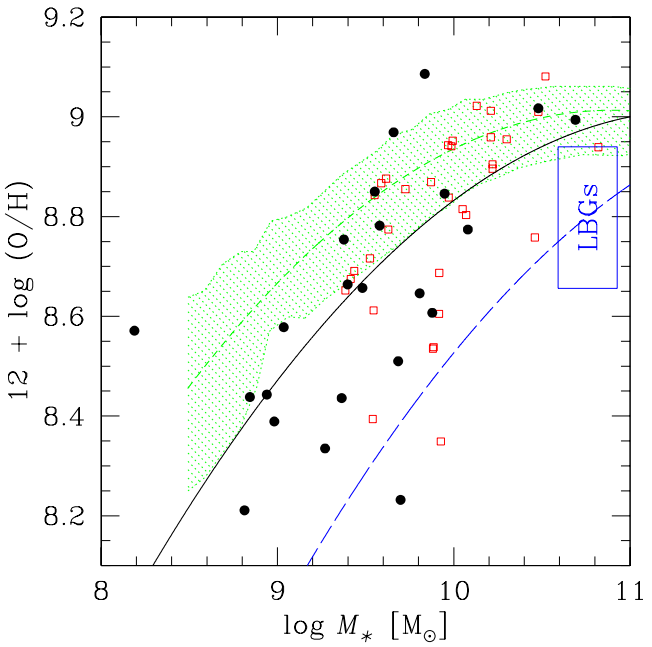

FIG. 13.— Metallicity as a function of stellar mass for GDDS (filled circles) and CFRS (open squares). The points are as in Figure 12, but error bars are omitted. The green short-dashed line and hatched area indicate the polynomial fit and $\pm 1\sigma$ dispersion, respectively, derived for the SDSS $z \sim 0.1$ galaxies (T04). The blue rectangle is the region occupied by the LBGs at $2.1 < z < 2.4$ (Shapley et al. 2004) after correcting from the N2 to the R_{23} calibrator. The black-solid and blue long-dashed lines are the SDSS polynomial shifted to the right to match the galaxy distributions at $z \sim 0.7$ and $z \sim 2.3$, respectively.

dian diameter of 4.6 kpc (T04). At a distance of 4.6/2 kpc from the center, according to Rolleston et al. (2000), the abundance of the Milky Way is 9.2, and higher if one takes the mean abundances in the inner region. Thus it is not surprising that SDSS galaxies have high metallicities.

In the following subsections we show that other possible systematic effects are not going to dramatically change our conclusions on the evolution of the M-Z relation.

8.1. *Aperture effects*

If there is a gradient of the metallicity with the distance from the center (Vila-Costas & Edmunds 1992; Zaritsky, Kennicutt & Huchra 1994; Garnett et al. 1997; Rolleston et al. 2000), it is important to make sure that this effect is not dominating when comparing samples obtained using different slit apertures.

We considered that the central part of a galaxy is more luminous than the outer part, and at high redshift is going to dominate the signal in the spectra. Kewley et al. (2005) have investigated the aperture effects as a function of redshifts, and found that the metallicity is generally not more than 0.1 dex larger than the average in the ~ 4 kpc central region. This 4 kpc corresponds to an angular size $< 0.8''$ for galaxies at $z > 0.4$. For this reason, the aperture effects are not strongly affecting the $z \sim 0.7$ results, because the region probed is generally large enough, and because residual offsets are affecting galaxies in a similar way.

The SDSS fiber aperture corresponds to a median projected diameter of 4.6 kpc (circular area is 16.6 kpc^2), with a range extending from 1 to 12 kpc^2, from the low to the high redshift end. However, T04 estimated a modest (0.1 dex) metallicity change in the same redshift interval. The GDDS extraction aperture rectangle is 0.75×0.8 arcsec^2 and corresponds to 3.9×4.2 kpc^2 and 5.9×6.3 kpc^2, from $z = 0.38$ to 0.96. The median for the sample is 5.6×5.9 kpc^2. The dispersion of the physical area in the SDSS sample is higher than in GDDS, and the median value is lower. It is hard to estimate precisely the mean difference between the two apertures due to the large aperture dispersion in the SDSS, we do not expect the aperture effect to be important.

For the CFRS sample, the slit aperture is twice the GDDS aperture in the dispersion direction (1.3 arcsec, or 9.3 kpc at $z = 0.7$) and $20''$ in the perpendicular direction, so the galaxy area probed is larger than the SDSS area. However, following Kewley et al. (2005) and considering the small metallcity dispersion observed in the SDSS sample, we expect the effect to be small.

Another related effect is the galaxy inclination. T04 estimated 0.2 dex higher metallicity in fully face-on galaxies than in fully edge-on galaxies, for fixed mass. For 15 of our GDDS galaxies we obtained HST/ACS F814W images (Abraham et al., in preparation). One-third are face-on, 1/3 are edge-on and 1/3 are intermediate (Figure 6). Because this is a random effect, it would make the dispersion in the metallicity larger, but any significant difference between the $z \sim 0.1$ and the $z \sim 0.7$ samples would remain basically unchanged.

8.2. *Different metallicity calibrators*

A very important systematic effect to take into account is linked to the several metallicity calibrators used by different studies. Kennicutt et al. (2003) showed that the metallicity based on an electron-temperature sensitive method is on average a factor of 2.5 lower than that derived using the empirical method by Kewley & Dopita (2002). This factor becomes ~ 2, when compared with the calibrator used by us (KK04).

We do not discuss here what the best method is, because this is still controversial and is a strong function of what is observationally available (e.g., what set of emission lines are used). However, because of these differences, we have paid particular attention to comparing metallicities after converting to the *same calibrator*, namely, the KK04 one. This is the minimum requirement necessary to make the detection of the redshift evolution of the M-Z relation more robust.

8.3. *Dust extinction correction*

Another possible bias to consider is the dust extinction. As stated in §3.2, dust extinction does not have a huge effect on the metallicity. This decreases by only 0.2 dex if A_V goes from 0 to 3. We applied $A_V = 2.1$ and $A_V = 1$ for GDDS and CFRS galaxies, respectively. The choice of using a lower extinction in the CFRS is justified by the higher luminosity of the CFRS galaxies, not entirely accounted for by the relatively higher stellar masses of the same sample with respect to the GDDS sample. Indeed, the CFRS is a R selected survey that used the 4m Canada-France-Hawaii Telescope, thus CFRS very likely could not identify highly extincted galaxies. The GDDS is a K selected survey that used a larger telescope, so suffers less from this bias.

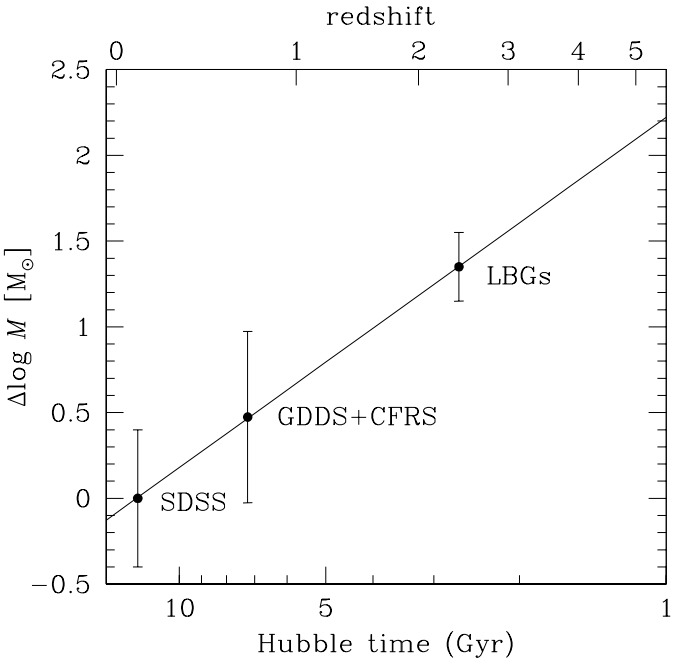

FIG. 14.— The points show the displacement in mass applied to the SDSS M-Z relation (for which $\Delta \log M \equiv 0$ by definition) to match the GDDS+CFRS and LBG distributions. This describes how much more massive a high-z galaxy with a given metallicity would roughly be with respect to local galaxies with similar metallicities. The error bars indicate the $\sim 1\sigma$ mass *dispersion* at the median metallicity in the samples, as seen in Figure 13. The small error bar for the LBGs is the effect of the small sample. The straight line is the linear correlation of the three points (Eq. 9).

Brinchman et al. (2004) found that massive (10^{10} $M_\odot < M_\star < 10^{11}$ $M_\odot$) star-forming galaxies on average suffer 3 times (in magnitudes) more extinction than low mass galaxies (10^8 $M_\odot < M_\star < 10^9$ $M_\odot$), i.e., opposite to what we have assumed. Even if there was no bias in the CFRS sample, assuming a larger extinction in the more massive galaxies would have a small effect on the correlation, but the scatter would be larger.

9. MODELING THE MASS-METALLICITY RELATION EVOLUTION

9.1. *An empirical model*

We now attempt to derive an empirical model describing the redshift evolution of the mass-metallicity relation. This will allow to predict the stellar mass (or the metallicity) of a galaxy at a given redshift and metallicity (or stellar mass).

Let us arbitrarily assume that at high redshift the shape of the SDSS relation is preserved, but it moves towards higher masses. We prefer to move the SDSS relation in the x direction instead of the y direction, because this can better reproduce $z \sim 0.7$ GDDS and CFRS points in the M-Z plane. The best match is obtained if the M-Z relation is moved to the right by $\Delta \log M \simeq 0.47$ (black solid curve in Figure 13). At higher redshift only the few galaxies studied by Shapley et al. (2004) have measured mass and metallicity, and these are represented by the rectangle in Figure 13. We have corrected metallicities in order to take into account systematic effects. Shapley et al. (2004) have used the N2 calibrator, which saturates for high metallicities (Pettini & Pagel 2004). If we again assume that the shape of the M-Z relation is preserved, the curve intercepts the locus of the LBG points for $\Delta \log M \simeq 1.35$. This mass displacement, the one at $z \sim 0.7$, and the SDSS point for which $\Delta \log M \equiv 0$, are shown in the plane t_H - $\Delta \log M$ (t_H is the Hubble time) of Figure 14. These three points are basically aligned along the straight line (also shown)

$$\Delta \log M(t_H) = -2.0436 \log t_H + 2.2223 \qquad (9)$$

in the $\log - \log$ space. If we combine Eq. 9 with Eq. 8, we derive the general relation that gives the metallicity of a galaxy at a given stellar mass and Hubble time:

$$12 + \log(\mathrm{O/H}) = -2.4412 + 2.1026[\log M_\star + \\ -\Delta \log M(t_H)] - 0.09649[\log M_\star - \Delta \log M(t_H)]^2 \qquad (10)$$

which is equivalent to:

$$12 + \log(\mathrm{O/H}) = -7.5903 + 2.5315 \log M_\star + \\ -0.09649 \log^2 M_\star + 5.1733 \log t_H - 0.3944 \log^2 t_H + \\ -0.4030 \log t_H \log M_\star \qquad (11)$$

Eq. 11 is shown in Figure 15, and predicts that low mass galaxies have a steeper redshift evolution in metallicity than bigger galaxies. Of course we have to consider the big uncertainty due to the way metallicities are measured. However, Eq. 11 describes in a simple and powerful fashion the evolution of the metal cosmic abundance in the Universe for different mass bins. It predicts the mean metallicity of galaxies at a given mass and redshift, but does not give the time evolution of a single galaxy. This is done in the next section.

9.2. *A closed-box model*

A qualitative explanation of the redshift evolution of the M-Z relation (Figure 15) is provided by a SFR which stops earlier in more massive galaxies than in low-mass galaxies (Heavens et al. 2004; Juneau et al. 2005). Another way to describe this is a gas fraction (gas mass over total mass) available for star formation, that declines more rapidly in more massive galaxies, or a period of star formation that lasts longer in less massive galaxies.

Theoretical scenarios explaining these observations, must properly consider gas flows in both directions (in and out of the galaxy). Galactic flows are mainly driven by the formation of massive stars which blow out gas from the galaxy, and by the gravitational potential of the galaxy (related to its mass), which on the one hand confines the gas in the galaxy, and on the other attracts metal-poor gas from the external IGM. The chemical evolution of galaxies over cosmic times was predicted by Pei & Fall (1995) using infall, outflow and closed-box (no flows) models. Larson (1974) described in his early work that low mass galaxies are metal poor due to the gas loss after supernova explosions. Ferrara & Tolstoy (2000) found later on in their models that indeed galaxies with gas mass $M_{gas} < 10^9$ $M_\odot$ lose mass in outflows.

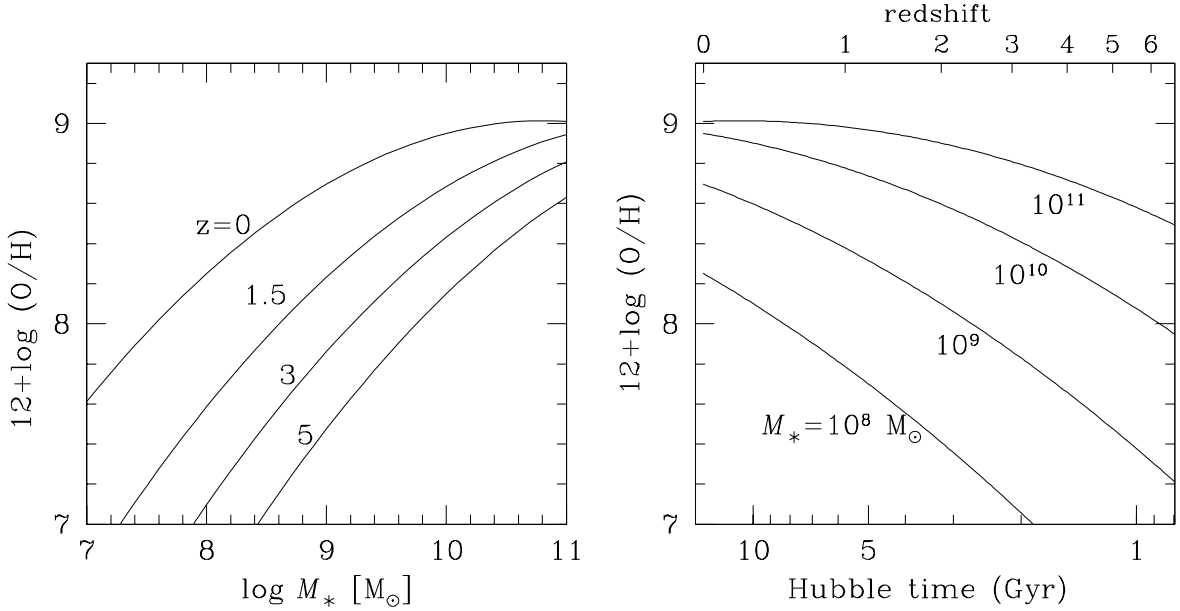

FIG. 15.— $12 + \log(O/H)$ as a function of stellar mass for constant redshifts (*left panel*), or as a function of Hubble time for constant stellar masses (*right panel*). These relations are obtained by extrapolating at all redshifts the $z \sim 0.1$ SDSS and our $z \sim 0.7$ M-Z relations. We emphasize that this empirical model is derived using the KK04 metallicity calibrator and BG03 IMF, and is different if other calibrators and IMFs are used.

We tried to reproduce the M-Z relation evolution using the closed-box approach. Although the large dispersion in the M-Z point distribution can indicate that galactic flows play a role in the chemical state of galaxies, the closed-box model allows one to start to understand what basic assumptions are necessary to explain the observations. We use the PÉGASE modeling (Fioc & Rocca-Volmerange 1997, 1999) and assume that initially the galaxy is only made of gas with a given total mass M_{tot} and zero metallicity. As the gas collapses and stars form, the total mass remains constant, and part of the gas is turned into stars. Both stellar mass and metallicity increase simultaneously as the galaxy evolves. The other key assumption is an exponential star formation SFR $\propto \exp^{-t/\tau}$, with an e-folding time τ proportional to the total baryonic mass of the galaxy, according to the following empirical relation:

$$\log \tau = a \log M_{tot} + b \qquad (12)$$

For $a < 0$, the SFR declines more rapidly in more massive galaxies. We tune this equation to reproduce the proposed M-Z relation evolution of Eq. 11 and Figure 13. This occurs for $a = -0.88$ and $b = 9.42$ (small insert in Figure 16). The results of the model, assuming a redshift of formation $z_f = 3.5$, are shown by the dotted lines in Figure 16; they are not very sensitive to z_f, if this is in the range $z_f = 3 - 1000$. A galaxy with a stellar mass of $10^{8.0}$ $M_\odot$ at $z = 2.3$ will have a stellar mass of $10^{8.8}$ $M_\odot$ at $z = 0.1$, i.e. a factor of 6 higher than 9.5 Gyr before ($z = 2.3$). Another galaxy with stellar mass $10^{9.7}$ $M_\odot$ at $z = 2.3$, will only have doubled its stellar mass after the same time interval has passed. The increase in metallicity is a factor of 10 in the less massive galaxy, and only a factor of 3 in the more massive galaxy. This simple model, where τ is a function of the mass, provides a good explanation of the observed results. Without any variation of τ, it is not possible to account for the M-Z relation at $z \sim 0.1$, and all galaxies would have solar metallicity, regardless of mass and redshift of formation (if in the range $z_f = 3 - 1000$).

10. DISCUSSION

The mass-metallicity (or the luminosity-metallicity) relation is a well known phenomenon identified in the local Universe in several surveys (Faber 1973; Lequeuex et al. 1979; Garnett & Shields 1987; Skillman, Kennicutt, & Hodge 1989; Zaritsky et al. 1994). Although any correlation is more difficult to detect at high redshift, due to the limited size of surveys, it is already clear that galaxies with a given luminosity are more metal poor than similarly luminous galaxies in the local Universe (Kobulnicky & Koo 2000; Pettini et al. 2001; Lilly et al. 2003; Liang et al. 2004; Shapley et al. 2004). Only recently it was possible to firmly establish that the relation between mass and luminosity persists at high redshift ($z \sim 0.7$; KK04), thanks primarily to the large sample of galaxies available (about 200 from TKRS) and to the large interval in luminosity spanned. Such a relation at high redshift is displaced with respect to the local relation.

All this is generally based on the B luminosity, a parameter that poorly constrains the galaxy mass, because the B luminosity is easily extincted by dust, and represents short-lived massive stars more than the bulk of the stellar mass. Stellar mass is a more meaningful galaxy parameter.

The stellar mass and metallicity of 56 galaxies in our sample ($0.4 < z < 1$) are correlated (at $\sim 6\sigma$ significance level). This relation is much stronger than the luminosity-metallicity relation for the same sample (for which the dispersion around the best fit is 65% higher), or for the TKRS sample at similar redshifts.

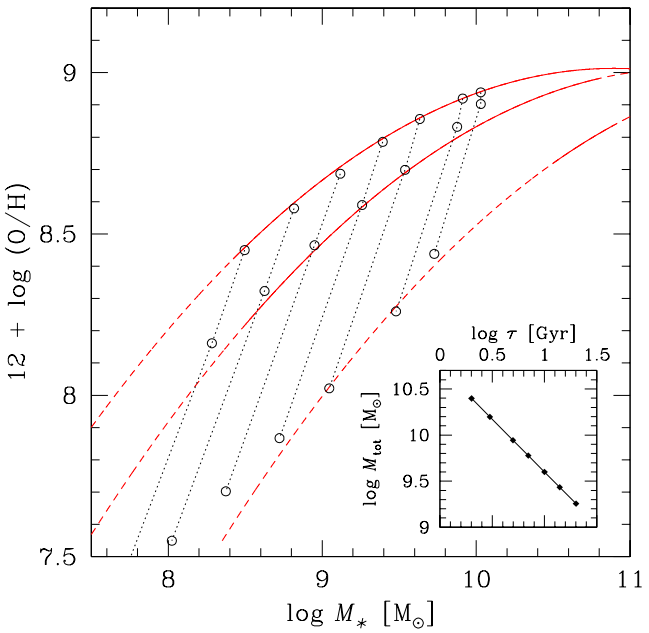

FIG. 16.— Closed-box model predictions of 12 + log(O/H) as a function of stellar mass (dotted lines), for redshift of formation $z_f = 3.5$, and for increasing values of the initial mass (from left to right). Results are not very sensitive to z_f, if this is in the range $z_f = 3-1000$. Open circles mark the three redshift epochs $z = 2.3$, 0.7 and 0.1, from bottom to top. The dashed and solid lines are results from observations at $z = 2.3$, 0.7 and 0.1 from bottom to top (as shown in Figure 13, see text). These lines are solid in the mass range covered by observations. The small insert shows the e-folding time as a function of the total galaxy mass adopted by the model, also described by Eq. 12 for $a = -0.95$ and $b = 10.6$. The mass intervals marked by the diamonds are as in the dotted lines of the M-Z relation.

This M-Z relation is displaced towards higher stellar masses, and/or lower metallicities, with respect to the $z \sim 0.1$ M-Z relation for SDSS star-forming galaxies. The rate at which mass and metallicity evolve with time can be estimated, also using results from the 7 $z \sim 2.3$ LBGs studied by Shapley et al. (2004). Although the $z \sim 2.3$ sample is too small to establish any relation between mass and metallicity, we used it to normalize a hypothetical M-Z relation at $z \sim 2.3$. Such an additional information is very important, because it doubles the time interval: the Universe at $z \sim 2.3$ is 4.6 Gyr younger than at $z \sim 0.7$, which is 4.9 Gyr younger than at $z \sim 0.1$. We assume that the shape of M-Z relation found at $z \sim 0.1$ does not change with time, and move it on the stellar-mass axis, to find the best match with the observed points at $z = 0.7$ and 2.3.

We parametrize this displacement of mass and derive a general relation for the metallicity that is a function of the stellar mass and of the Hubble time (Eq. 11 and Figure 15). With this generalized relation, we can statistically predict the mass of a galaxy at a given redshift and metallicity. Eq. 11 describes in a simple and powerful fashion the evolution of the cosmic metal abundance as a function of the galaxy stellar mass. It can also be used to test predictions of semi-analytic models (Somerville, Primack & Faber 2001), analytic models (Pei, Fall & Hauser 1999), or numerical simulations (Nagamine et al. 2004).

Any attempt to detect any cosmic chemical evolution would fail if this is done combining galaxies with very different stellar masses. Our empirical model indicates that massive galaxies evolve in terms of metallicity more slowly than less massive galaxies. The DLAs offer the opportunity to investigate consistently the chemical evolution for a particular class of galaxies over a large fraction of the cosmic time. It is now commonly accepted that DLAs do show chemical evolution (Prochaska et al. 2003). This evolution can be compared with our predictions to derive the stellar masses of DLA galaxies. Of course, big uncertainties can lead to systematic errors. For instance, it is hard to estimate any systematic difference between the metallicity derived from absorption lines and emission lines. Moreover, statistically, DLAs are tracing the outskirt of galaxies (Chen et al. 2005) where metallicity is generally lower than the metallicity in the central star-forming region (Ellison et al. 2005). Chen et al. (2005) estimated a metallicity gradient of 0.041 ± 0.012 dex kpc^{-1}.

We compared DLA observations to our empirical model, after applying to the model a constant negative correction in metallicity of 0.3 dex. Such an assumption is justified by assuming a typical impact parameter of the DLA from the galaxy center of 10 kpc, and considering that our empirical relation is derived from galaxies observed over a region that is on average about 7 kpc across. We take the mean metallicity in redshift bins derived from a sample of 87 DLAs after dust depletion correction (Savaglio 2001). This is similar to the one more recently derived by Prochaska et al. (2003) using 100 DLAs. The result is shown in Figure 17. Remarkably, the best fit predicts that the stellar mass of DLA galaxies is $M_\star = 10^{8.82\pm0.65}$ $M_\odot$, all the way from $z \sim 0.5$ to 4.1. This suggests that typical DLAs are not originating in very low-mass dwarf galaxies, but are intermediate mass systems. The estimated stellar mass would be 2 times higher (+0.3 dex) if the metallicity derived using the R_{23} parameter is overestimated by a factor of 2 (Kennicutt et al. 2003; KK04).

Figure 15 and Eq. 11 also suggests that local dwarf star-forming galaxies, with metallicities of $\sim 1/10$ solar (Aloisi et al. 2003; and references therein), have stellar masses of the order of 10^7 $M_\odot$. In the distant Universe, the star-forming galaxies at $z \sim 2.1$ of the K20 with stellar masses (after correcting for BG03 IMF) of $\sim 10^{11}$ $M_\odot$ (Fontana et al. 2004) would have a mean metallicity slightly over solar, in agreement with results derived using UV stellar features by de Mello et al. (2004). In a previous GDDS work (Savaglio et al. 2004) we have studied the ISM absorption in a sample of 13 galaxies at mean redshift $z \sim 1.6$ and found indication of high metal enrichment. The average stellar mass of this sample is $M_\star = 10^{10.4}$ $M_\odot$, which leads again, according to Eq. 11, to metallicity slightly above solar.

For the LBGs studied by Pettini et al. (2001) at $z = 3-3.4$, applying the KK04 calibrator and a modest dust extinction of $A_V = 1$, the reported emission line fluxes of 4 galaxies give 12 + log (O/H) = 8.4 − 8.8. At the redshift of the galaxies, Eq. 11 gives a mean stellar mass of $M_\star = 10^{10.4}$ $M_\odot$, i.e. about a factor of 2 less massive than the mean value in the $z \sim 2.3$ LBGs of Shapley et al. (2004).

Massive LBGs are often used to derive the high-z SFR history of the Universe (the Madau plot; Madau et al.

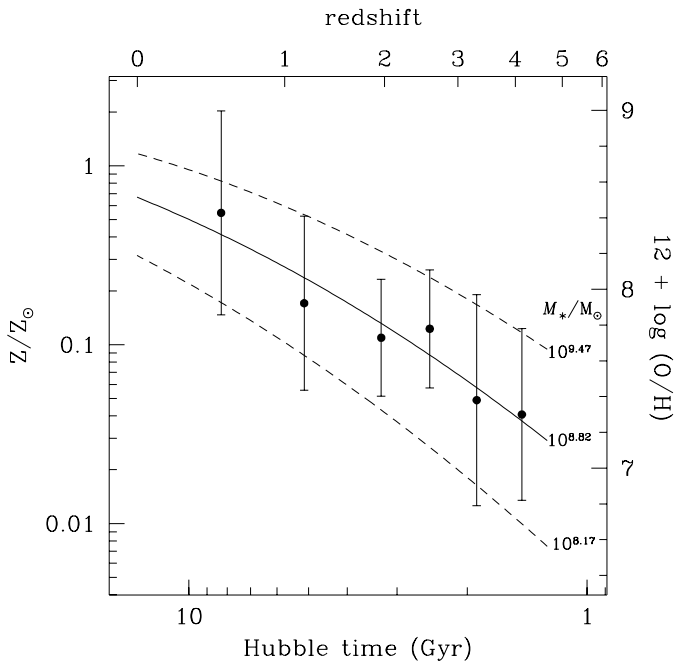

FIG. 17.— Comparison between mean metallicity in DLAs for different redshift bins (Savaglio 2001), and our empirical model of Eq. 11. The best fit gives a stellar mass for DLAs of $10^{8.82}$ $M_\odot$ (solid line) with a dispersion of 0.65 dex (dashed lines). In this figure we made a correction of −0.3 dex to the model to account for a metallicity gradient in DLAs (Chen et al. 2005). The best-fit mass would be 0.3 dex higher if the R_{23} metallicity, used to calibrate the empirical model, is underestimated by a factor of 2 (Kennicutt et al. 2003).

1996). The Madau plot is then used to derive the cosmic chemical evolution. A discrepancy with the DLA metallicity evolution (which is lower and steeper) was noticed by Madau, Pozzetti, & Dickinson (1998). The discrepancy is likely because the metallicity evolution of different galaxies with substantially different stellar masses are compared. This is confirmed by by Hopkins, Rao, & Turnshek (2005), who found that DLAs have a dominant role in the SFR density only in the late Universe ($z < 0.6$), but at higher redshift their contribution is much less important. We also note that even if the analytic model of the cosmic metallicity evolution by Pei et al. (1999) resembles the DLA metallicity evolution, this alone does not necessarily prove that the cosmic chemical evolution is well represented by the DLA galaxies.

Our empirical model can be tested using recent results on a DLA sample at $1.7 < z < 3.7$ (Ledoux et al. 2005) showing a correlation between FeII absorption equivalent width (representing the galaxy dynamical mass) and metallicity. Metal rich DLAs have larger FeII EW than metal poor DLAs, a result which is reminiscent of the M-Z relation. If properly translated, their correlation at a mean redshift of $z \sim 2.4$ is consistent with our M-Z relation (C. Ledoux, private communication).

The observed evolution of the M-Z relation can be reproduced by a closed-box scenario where the e-folding time is shorter for more massive galaxies. A star formation more concentrated in time in massive galaxies than in less massive galaxies is consistent with the "downsizing" scenario of galaxy formation. Other models cannot be ruled out by our simple approach.

One shortcoming of our simple model is that it makes no attempt to consider the impact of galaxy-galaxy mergers on the evolution. This is known to evolve rapidly with redshift (Le Fèvre et al. 2000). Mergers have the most dramatic effect when they are between galaxies of similar mass, and in many such cases the merger product will no longer be star-forming and hence not be included in these samples. The existence of a tight M-Z relation implies that an equal mass merger will shift galaxies to the right in Figure 16, the net effect will be to make the model tracks less steep. A model which included merging would then have to have a different form for $\tau - M_{tot}$ in order to compensate for this effect. A full treatment of merging would require a detailed semi-analytic (e.g., Springel et al. 2005) or hydrodynamical model (Nagamine et al. 2004) of galaxy formation which is beyond the scope of this work, though we believe the empirical relations we have discovered will greatly inform such a comparison. We note that it is much more straight-forward to compare stellar mass with metallicity as galaxies assemble in a model as one has to make less assumptions (e.g., about dust) than one does with a luminosity comparison.

11. SUMMARY

In this paper, we investigated for the first time the high-z mass-metallicity relation. We used galaxies from the GDDS and CFRS, for which stellar mass estimates were possible thanks to the available multi-band optical-NIR photometry (Crampton et al. 1995; Le Fèvre et al. 1995; Lilly et al. 1995; McCarthy et al. 2001; Chen et al. 2002).

The metallicity was measured using the R_{23} and O_{32} over a sample of star-forming galaxies at $0.4 < z < 1$. For the CFRS sample, we recalculated values measured by Lilly et al. (2003) using the recent calibrator provided by Kobulnicky & Kewley (2004). Stellar mass and metallicity are measured simultaneously for 56 galaxies.

Thanks to the large mass range, $M_\star = 10^{8.2} - 10^{10.8}$ $M_\odot$, and the size of the sample, we unambiguously detect a 6σ significant correlation between stellar mass and metallicity at $z \sim 0.7$ (Eq. 7). Such a M-Z relation is displaced with respect to the M-Z relation at $z \sim 0.1$, towards higher stellar masses, or lower metallicities. Galaxies at a given metallicity are more massive than galaxies in the local universe with similar metallicity. We attribute the origin of this to the redshift evolution of the mass-metallicity relation. Although the shape of the M-Z relation depends to some extend on the choise of the metallicity calibrator, our result on the evolution of the M-Z relation is robust, as all metallicities are estimated using the same calibrator.

The stellar mass is more tightly correlated to metallicity than the luminosity (the dispersion around the best fit is 1.6 times smaller). Moreover, the redshift evolution of the M-Z relation is more significant than the redshift evolution of the metallicity found in large samples of galaxies with different stellar mass.

We find the M-Z evolution to be more rapid in lower-mass galaxies indicating that they are still actively being constructed. In contrast the more massive galaxies have already reached solar metallicity at $z = 1$ indicating that the bulk of their star-formation has completed.

Based on the observed results, we derive an empirical

model for the evolution of the mass-metallicity relation as a function of redshift which works surprisingly well. From this, one can estimate the expected stellar mass of a galaxy at a given metallicity and redshift. If our model is correct, we predict that the stellar mass of DLAs is $M_\star = 10^{8.8\pm0.7}$ $M_\odot$ at any redshift. According to the same model, the few LBGs at ~ 3.1 studied by Pettini et al. (2001) may have stellar masses of the order of 2×10^{10} $M_\odot$. The predicted masses are ~ 2 times higher if the T_e-based metallicity calibrator is used (Kennicutt et al. 2003).

Our empirical model is nicely reproduced by a toy scenario of galaxy formation where the important prescription is a star formation that proceeds more rapidly in more massive galaxies, as described by the downsizing scenario for galaxy formation. Any more detailed model of galaxy formation must also reproduce the observed M-Z relation as a function of redshift.

Future programs can test our predictions. For instance, by measuring metallicities of galaxies with known masses in the $z \sim 1.5$ Universe. Galaxies of the GDDS and K20 (Fontana et al. 2004; Glazebrook et al. 2004) would be a suitable testbed to this goal. To measure metallicities, NIR spectroscopy would be required, not an easy, but possible, task for those faint galaxies. Stellar masses of DLAs can directly be measured by obtaining K band photometry of QSO fields. This can more efficiently be done using the NIR capabilities of *HST* over low-z targets, to limit the confusion with the QSO PSF. Alternately ground-based Adaptive Optics may advance to the point where this is possible with larger telescopes. Finally, our proposed model of star formation history of galaxies, which is a function of mass, can be compared with the SFR history of the Universe in mass bins (Juneau et al. 2004; Heavens et al. 2004).

The authors thank the anonymous referee, Duilia de Mello, Lisa Kewley and Christy Tremonti for invaluable comments. Cédric Ledoux & Christy Tremonti are acknowledged for providing results prior to publication. This paper is based on observations obtained at the Gemini Observatory, which is operated by the Association of Universities for Research in Astronomy, Inc., under a cooperative agreement with the NSF on behalf of the Gemini partnership: the National Science Foundation (United States), the Particle Physics and Astronomy Research Council (United Kingdom), the National Research Council (Canada), CONICYT (Chile), the Australian Research Council (Australia), CNPq (Brazil), and CONICET (Argentina). K.G. and S.S. acknowledge generous funding from the David and Lucille Packard Foundation. H.–W.C. acknowledges support by NASA through a Hubble Fellowship grant HF-01147.01A from the Space Telescope Science Institute, which is operated by the Association of Universities for Research in Astronomy, Incorporated, under NASA contract NAS5-26555.

REFERENCES

Abraham, R. G. et al. 2004, AJ, 127, 2455
Allende Prieto, C., Lambert, D. L., & Asplund, M. 2001, ApJ, 556, L63
Aloisi, A., Savaglio, S., Heckman, T. M., Hoopes, C. G., Leitherer, C., & Sembach, K. R. 2003, ApJ, 595, 760
Aragon-Salamanca, A., Ellis, R. S., Couch, W. J., & Carter, D. 1993, MNRAS, 262, 764
Baldry, I. K. & Glazebrook, K. 2003, ApJ, 593, 258
Bresolin1, F., Schaerer, D., González Delgado, R. M., & Stasińska, G. 2005, A&A, in press (astro-ph/0506088)
Brinchmann, J., Charlot, S., White, S. D. M., Tremonti, C., Kauffmann, G., Heckman, T., & Brinkmann, J. 2004, MNRAS, 351, 1151
Brinchmann, J., & Ellis R. S. 2000, ApJ, 536, L77
Bruzual, G., & Charlot, S., 2003, MNRAS, 344, 1000
Calzetti, D. 1997, AJ, 113, 162
Calzetti, D. 2001, PASP, 113, 1449
Chen, H.-W., et al. 2002, 570, 54
Chen, H.-W., Kennicutt, R. C., Rauch, M. 2005, ApJ, 620, 703
Cid Fernandes, R., Mateus, A., Sods, L., Stasińska, G., Gomes, J. M. 2005, MNRAS, 358, 363
Crampton, D., Le Fèvre, O., Lilly, S. J., & Hammer, F. 1995, ApJ, 455, 96
Cuillandre, J. C., et al. 1994, A&A, 281, 603
de Mello, D. F., Daddi, E., Renzini, A., Cimatti, A., di Serego Alighieri, S., Pozzetti, L., & Zamorani, G. 2004, ApJ, 608, L29
Denicoló, G., Terlevich, R., & Terlevich, E. 2002, MNRAS,
Dopita, M. A., & Evans, I. N. 1986, ApJ, 307, 431
Drory, N., Bender, R., & Hopp, U. 2004, ApJ, 616, L103
Edmunds, M. G., & Pagel, B. E. J. 1984, MNRAS, 211, 507
Faber, S. M. 1973, ApJ, 179, 731
Fioc, M. & Rocca-Volmerange, B. 1997, A&A, 326, 950
—. 1999, astro-ph/9912179
Ellison, S. L., Kewley, L. J., Mallen-Ornelas, G. 2005, MNRAS, 357, 354
Feigelson, E. D., & Babu, G. J. 1992, ApJ, 397, 55
Ferrara A. & Tolstoy E. 2000, MNRAS, 313 291
Fontana, A., et al. 2004, A&A, 424, 23
Garnett, D. R., & Shields, G. A. 1987, ApJ, 317, 82
Garnett, D. R., Shields, G. A., Skillman, E. D., Sagan, S. P., Dufou,r R. J. 1997, ApJ 489, 36
Glazebrook, K. & Bland–Hawthorn, J. 2001, PASP, 113, 197
Glazebrook, K., et al. 2003, ApJ, 587, 55
Glazebrook, K., et al. 2004, Nature, 430, 181
Heavens, A., Panter, B., Jimenez, R., & Dunlop, J. 2004, Nature, 428, 625
Hopkins, A. M., Rao, S. M., Turnshek, D. A. 2005, ApJ, in press (astro-ph/0505418)
Jansen, R. A., Fabricant, D., Franx, M., & Caldwell, N. 2000, ApJS, 126, 331
Juneau, S. et al. 2005, ApJ, 619, L135
Kennicutt, R. C. 1992, ApJ, 79, 255
Kennicutt, R. C. 1998, ApJ, 498, 541
Kennicutt, R. C., Bresolin, F., & Garnett, D. R. 2003, ApJ, 591, 801
Kewley, L. J., & Dopita, M. A. 2002, ApJS, 142, 35
Kewley L. J., Jansen, R. A., Geller, M. J. 2005, PASP, 117, 227
Kobulnicky, H. A., et al. ApJ, 2003, 599, 1006
Kobulnicky, H. A., Kennicutt, R. C., & Pizagno, J. L. 1999, ApJ, 514, 544
Kobulnicky, H. A., & Kewley L. J. ApJ, 2004, 617, 240
Kobulnicky, H. A., & Koo, D. C. 2000, ApJ, 545, 712
Kobulnicky, H. A., & Phillips, A. C. 2003, ApJ, 599, 1031
Kroupa, P. 2001, MNRAS, 322, 231
Larson, R. B. 1974, MNRAS, 169, 229
Le Fèvre, O., Crampton, D., Lilly, S. J., Hammer, F., & Tresse, L. 1995, ApJ, 455, 60
Le Fèvre, O., et al. 2000, MNRAS, 311, 565
Ledoux, C., Petitjean, P., Møller, P., Fynbo, J., Srianand, R. 2005, proceedings of IAU Colloquium No. 199 "Probing Galaxies through Quasar Absorption Lines", P.R. Williams, C. Shu, B. Menard, eds
Lequeux, J., Peimbert, M., Rayo, J. F., Serrano, A., & Torres-Peimbert, S. 1979, A&A, 80, 155
Liang, Y. C., Hammer, F., Flores, H., Elbaz, D., Marcillac, D., & Cesarsky, C. J. 2004, A&A, 423, 867
Lilly, S. J., Carollo, C. M., & Stockton, A. N. 2003, ApJ, 597, 730
Lilly, S. J., Le Fèvre, O., Crampton, D., Hammer, F., & Tresse, L. 1995, ApJ, 455, 50

Madau, P., Ferguson, H. C., Dickinson, M. E., Giavalisco, M., Steidel, C. C., & Fruchter, A. 1996, MNRAS, 283, 1388
Madau, P., Pozzetti, L., & Dickinson, M. 1998, ApJ, 498, 106
McCall, M. L., Rybski, P. M., & Shields, G. A. 1985, ApJS, 57, 1
McCarthy, P. J., et al. 2001, ApJ, 560, L131
McGaugh, S. S. 1991, ApJ, 380, 140
Nagamine, K., Springel, V., & Hernquist, L. 2004, MNRAS, 348, 435
Osterbrock, D. E. 1989, Astrophysics of Gaseous Nebulae and Active Galactic Nuclei (Mill Valley: University Science Books)
Pagel, B. E. J., Edmunds, M. G., Blackwell, D. E., Chun, M. S., & Smith, G. 1979, MNRAS, 189, 95
Pei, Y. C., & Fall, S. M. 1995, ApJ, 454, 69
Pei, Y. C., Fall, S. M., & Hauser, M. G. 1999, ApJ, 522, 604
Pettini, M., & Pagel, B. E. J. 2004, MNRAS, 348, L59
Pettini, M., Shapley, A. E., Steidel, C. C., Cuby, J., Dickinson, M., Moorwood, A. F. M., Adelberger, K. L., & Giavalisco, M. 2001, ApJ, 554, 981
Pettini, M., Steidel, C. C., Adelberger, K. L., Dickinson, M., & Giavalisco, M. 2000, ApJ, 528, 96
Pilyugin, L. S. 2001, A&A, 369, 594
Portinari, L., Sommer-Larsen, J., & Tantalo, R. 2004, MNRAS, 347, 691
Prochaska, J. X., Gawiser, E., Wolfe, A. M., Castro, S., & Djorgovski, S. G. 2003, ApJ, 595, L9
Rolleston, W. R. J., Smartt, S. J., Dufton, P. L., & Ryans, R. S. I. 2000, A&A, 363, 537
Salpeter, E. E. 1955, ApJ, 121, 161
Savaglio, S. 2001, IAU Symposium, 204, 307
Savaglio, S., et al. 2004, ApJ, 602, 51
Schade, D., Carlberg, R. G., Yee, H. K. C., Lopez-Cruz, O., & Ellingson, E. 1996, ApJ, 465, L103
Schulte-Ladbeck, R. E., König, B., Miller, C. J., Hopkins, A. M., Drozdovsky, I. O., Turnshek, D. A., Hopp, U., 2005, ApJL, 625, L79
Shapley, A. E., Erb, D. K., Pettini, M., Steidel, C. C., Adelberger K. L. 2004, ApJ, 612, 108
Skillman, E. D., Kennicutt, R. C., & Hodge, P. W. 1989, ApJ, 347, 875
Somerville, R. S., Primack, J. R., & Faber, S. M. 2001, MNRAS, 320, 504
Spergel, D. N., et al. 2003, ApJS, 148, 175
Springel, V., et al. 2005, Nature, 435, 629
Tremonti, C. A., et al. 2004, ApJ, 613, 898
Vila-Costas, M. B., & Edmunds, M. G. 1992, MNRAS, 259, 121
Vogt, N. P., Forbes, D. A., Phillips, A. C., Gronwall, C., Faber, S. M., Illingworth, G. D., & Koo, D. C. 1996, ApJ, 465, L15
Wirth, G. D., et al. 2004, AJ, 127, 3121
Zaritsky, D., Kennicutt, R. C., & Huchra, J. P. 1994, ApJ, 420, 87

Table 1. GDDS galaxies

ID	z	$f_{[OII]3727}$[a]	$f_{H\gamma}$[a,b]	$f_{H\beta}$[a,b]	$f_{[OIII]4959}$[a]	$f_{[OIII]5007}$[a]	$\log R_{23}$[c]	$\log O_{32}$[c]	$12+\log(O/H)$[d]	V[e]	z'[e]	K[e]	$M_{B,AB}$	$\log M_\star$[f]
SA02-0585	0.826	15.52 ± 0.69	1.98 ± 1.04	5.21 ± 1.40	3.05 ± 1.21	16.78 ± 1.16	0.95 ± 0.12	-018 ± 0.06	8.389 ± 0.235	23.76	22.57	> 20.6	-19.96	8.98 ± 0.09
SA02-0756	0.864	11.03 ± 0.59	1.33 ± 0.49	2.69 ± 0.82	2.99 ± 1.11	8.97 ± 1.94	1.06 ± 0.14	-0.25 ± 0.10	8.211 ± 0.343	24.75	23.48	> 20.6	-19.10	8.81 ± 0.38
SA12-5685	0.961	16.47 ± 0.46	...	10.72 ± 2.11	...	20.29 ± 2.52	0.71 ± 0.09	-0.07 ± 0.06	8.754 ± 0.099	23.82	22.84	20.12	-20.71	9.38 ± 0.13
SA12-5722	0.842	6.35 ± 0.76	...	7.55 ± 2.02	...	5.32 ± 0.78	0.38 ± 0.12	-0.24 ± 0.08	8.994 ± 0.058	24.52	22.39	18.37	-20.43	10.69 ± 0.10
SA12-7099	0.567	6.97 ± 0.65	...	12.60 ± 0.46	...	< 2.0	0.02 ± 0.06	-1.30 ± 0.65	> 9.1	23.01	20.88	17.54	-20.09	10.63 ± 0.08
SA12-7205	0.567	6.31 ± 0.49	...	8.31 ± 0.32	...	< 1.4	0.20 ± 0.05	-0.82 ± 0.14	> 9.1	23.50	22.10	19.13	-19.41	9.86 ± 0.25
SA12-7660	0.791	10.89 ± 0.40	3.92 ± 0.41	10.85 ± 0.60	...	2.23 ± 0.89	0.32 ± 0.05	-0.85 ± 0.14	9.017 ± 0.020	23.91	22.01	18.53	-20.56	10.48 ± 0.14
SA12-7939	0.664	5.79 ± 0.31	0.91 ± 0.27	2.09 ± 0.30	2.33 ± 0.28	5.30 ± 0.50	0.92 ± 0.07	-0.17 ± 0.06	8.438 ± 0.125	24.38	23.23	> 20.6	-18.94	8.84 ± 0.05
SA12-8250	0.766	5.80 ± 0.40	...	3.42 ± 0.47	...	2.35 ± 0.69	0.59 ± 0.07	-0.56 ± 0.11	8.850 ± 0.064	24.57	> 23.5	20.64	-19.39	9.55 ± 0.34
SA15-4272	0.918	10.08 ± 0.26	...	3.47 ± 1.41	4.93 ± 1.32	17.55 ± 1.11	1.05 ± 0.18	0.06 ± 0.06	8.276 ± 0.417	24.96	22.99	> 20.6	-19.32	10.10 ± 0.31
SA15-4662	0.895	8.83 ± 0.26	2.68 ± 0.25	8.35 ± 0.59	...	4.99 ± 0.98	0.42 ± 0.05	-0.41 ± 0.08	8.969 ± 0.025	25.18	23.25	20.47	-19.30	9.66 ± 0.29
SA15-5596	0.890	24.47 ± 0.37	2.71 ± 0.35	7.84 ± 0.67	...	16.12 ± 1.87	0.91 ± 0.05	-0.34 ± 0.06	8.443 ± 0.087	24.18	23.07	> 20.6	-19.66	8.94 ± 0.29
SA15-6565	0.955	23.78 ± 0.53	3.86 ± 0.49	13.50 ± 1.94	10.97 ± 2.19	34.66 ± 3.25	0.80 ± 0.07	-0.01 ± 0.06	8.646 ± 0.092	24.68	23.29	> 20.6	-19.13	9.81 ± 0.47
SA15-7399	0.621	1.79 ± 0.33	...	< 1.5	1.97 ± 0.30	4.43 ± 0.32	0.79 ± 0.16	0.26 ± 0.10	< 8.7	> 26.3	> 23.5	> 20.6	-17.34	...
SA22-0040	0.818	22.74 ± 0.45	...	8.82 ± 1.60	9.89 ± 1.11	26.61 ± 1.06	0.93 ± 0.08	-0.08 ± 0.05	8.436 ± 0.150	23.78	22.60	20.28	-19.80	9.36 ± 0.40
SA22-0145	0.753	19.29 ± 0.56	...	8.81 ± 0.74	7.91 ± 0.79	17.45 ± 1.52	0.82 ± 0.04	-0.17 ± 0.05	8.607 ± 0.065	23.72	22.42	20.19	-19.50	9.88 ± 0.24
SA22-0563	0.786	32.69 ± 0.41	8.38 ± 0.69	17.63 ± 0.71	9.28 ± 1.15	15.79 ± 1.23	0.67 ± 0.03	-0.40 ± 0.05	8.782 ± 0.035	23.17	22.04	19.71	-20.42	9.58 ± 0.21
SA22-0619	0.671	3.64 ± 0.20	...	1.89 ± 0.17	...	1.89 ± 0.27	0.68 ± 0.05	-0.45 ± 0.07	8.774 ± 0.057	24.82	22.77	19.37	-18.74	10.08 ± 0.27
SA22-0630	0.753	4.81 ± 0.42	4.88 ± 0.36	14.50 ± 0.66	2.74 ± 0.61	7.83 ± 1.79	0.11 ± 0.05	0.05 ± 0.10	9.086 ± 0.012	23.61	21.63	19.07	-20.26	9.84 ± 0.26
SA22-0643	0.787	7.63 ± 0.39	...	2.91 ± 0.58	...	2.37 ± 0.98	0.76 ± 0.10	-0.67 ± 0.15	8.664 ± 0.131	23.95	22.70	20.28	-19.65	9.40 ± 0.35
SA22-0751	0.471	20.69 ± 0.70	...	7.60 ± 0.33	3.83 ± 0.42	11.15 ± 0.46	0.83 ± 0.04	-0.43 ± 0.05	8.578 ± 0.054	23.31	22.12	20.42	-18.62	9.04 ± 0.26
SA22-0926	0.785	8.55 ± 0.51	...	4.61 ± 1.04	4.91 ± 1.15	9.03 ± 1.54	0.79 ± 0.10	-0.08 ± 0.08	8.657 ± 0.140	24.07	22.65	> 20.6	-19.45	9.48 ± 0.53
SA22-0997	0.642	8.33 ± 0.52	...	2.12 ± 0.66	2.11 ± 0.43	7.49 ± 0.37	1.05 ± 0.14	-0.23 ± 0.06	8.232 ± 0.339	24.71	22.97	> 20.6	-18.12	9.70 ± 0.13
SA22-1534	0.469	2.84 ± 0.57	...	< 0.9	...	1.95 ± 0.39	0.94 ± 0.19	-0.33 ± 0.12	< 8.4	24.54	23.03	> 20.6	-17.31	8.37 ± 0.47
SA22-1674	0.879	19.36 ± 0.37	3.32 ± 0.35	9.33 ± 0.65	10.64 ± 1.59	30.31 ± 1.21	0.89 ± 0.04	0.04 ± 0.05	8.510 ± 0.061	24.52	> 23.5	> 20.6	-19.24	9.69 ± 0.57
SA22-2196	0.627	8.98 ± 0.52	...	2.75 ± 0.74	3.73 ± 0.52	8.57 ± 0.49	1.00 ± 0.12	-0.15 ± 0.06	8.335 ± 0.261	24.75	> 23.5	> 20.6	-18.28	9.27 ± 0.65
SA22-2491	0.470	7.23 ± 0.65	...	3.51 ± 0.30	3.40 ± 0.41	9.32 ± 0.48	0.85 ± 0.05	$-.04 \pm 0.06$	8.571 ± 0.073	24.05	22.67	> 20.6	-17.78	8.19 ± 0.44
SA22-2541	0.617	8.01 ± 0.48	...	4.83 ± 0.70	1.33 ± 0.54	3.77 ± 0.43	0.60 ± 0.07	-0.49 ± 0.08	8.846 ± 0.064	23.33	21.52	18.78	-19.75	9.95 ± 0.42

[a]Fluxes, in 10^{-18} erg s^{-1} cm^{-2}, are not corrected for dust extinction.
[b]Corrected for Balmer stellar absorption.
[c]Corrected for dust extinction assuming $A_V = 2.1$.
[d]Errors do not include systematic uncertainties.
[e]Vega magnitudes from LCIRS.
[f]Stellar masses in units of solar masses.

TABLE 2
GDDS COMPOSITE EMISSION LINE FLUXES

Line ratio	Measured	Theory [a]		A_V [b]	
		10^4 K	5000 K	10^4 K	5000 K
Hγ/Hβ	0.292 ± 0.026	0.470	0.458	3.47 ± 0.64	3.28 ± 0.64
Hδ/Hβ	0.180 ± 0.017	0.262	0.250	1.91 ± 0.48	1.67 ± 0.48
Hϵ/Hβ	0.127 ± 0.018	0.159	0.153	1.00 ± 0.61	0.83 ± 0.61
H8/Hβ	0.035 ± 0.016	0.107	0.102	4.57 ± 1.89	4.37 ± 1.89
[OII]/Hβ	2.280 ± 0.081	. . .	. . .	. . .	. . .
[OIII]λ5007/Hβ	2.262 ± 0.088	. . .	. ..	. . .	. . .
[OIII]λ4959/Hβ	0.647 ± 0.042	. . .	. . .	. . .	. . .
[OIII]λ4363/Hβ	< 0.03	. . .	. . .	. . .	. . .
[NeIII]/Hβ	0.208 ± 0.024	. . .	. . .	. . .	. . .
			Weighted mean	2.13 ± 0.32	1.92 ± 0.32

[a] As expected from atomic physics, for two temperatures, and assuming no dust extinction.
[b] Visual extinction, given the observed flux ratio and assuming two temperatures.

TABLE 3
CFRS SAMPLE

ID	z	K	$M_{B,AB}$[a]	$12+\log(\mathrm{O/H})$		$\log M_\star$
		(mag)	(mag)	LCS	This paper[b]	[$M_\odot$]
03.0062	0.826	20.17 ± 0.13	-22.30	9.10	> 9.06	10.57 ± 0.19
03.0085	0.609	21.32 ± 0.39	-20.40	8.84	8.88 ± 0.04	9.62 ± 0.35
03.0125	0.789	20.89 ± 0.21	-21.02	8.94	8.96 ± 0.05	10.21 ± 0.19
03.0145	0.603	21.20 ± 0.28	-20.87	8.74	8.77 ± 0.06	9.63 ± 0.20
03.0261	0.697	20.18 ± 0.11	-20.95	8.74	8.76 ± 0.06	10.46 ± 0.14
03.0327	0.609	20.71 ± 0.22	-20.49	8.92	8.95 ± 0.07	9.99 ± 0.27
03.0488	0.605	21.31 ± 0.38	-20.89	8.64	8.69 ± 0.07	9.44 ± 0.28
03.0570	0.646	21.79 ± 0.60	-20.51	8.64	8.68 ± 0.10	9.42 ± 0.57
03.0595	0.605	20.65 ± 0.21	-20.92	8.90	8.94 ± 0.05	9.99 ± 0.19
03.0599	0.479	21.25 ± 0.36	-20.66	8.30	8.39 ± 0.22	9.54 ± 0.25
03.0879	0.601	...	-19.94	8.90	8.94 ± 0.04	...
03.0999	0.706	19.93 ± 0.11	-21.57	8.94	> 8.94	10.51 ± 0.20
03.1016	0.702	21.29 ± 0.38	-20.49	8.80	8.84 ± 0.04	9.97 ± 0.46
03.1112	0.768	...	-21.00	8.56	8.61 ± 0.10	...
03.1138	0.768	21.61 ± 0.51	-20.70	8.56	8.63 ± 0.08	...
03.1309	0.617	19.32 ± 0.05	-21.86	8.94	8.94 ± 0.06	10.82 ± 0.14
03.1349	0.617	19.29 ± 0.05	-21.57	8.98	9.01 ± 0.03	10.48 ± 0.35
03.1367	0.703	...	-20.78	8.80	8.84 ± 0.05	...
03.1375	0.635	23.29 ± 2.37	-20.43	8.84	8.88 ± 0.07	...
03.1534	0.794	...	-20.75	8.58	8.63 ± 0.05	...
03.9003	0.618	...	-21.67	9.02	9.03 ± 0.03	...
10.0478	0.752	...	-21.42	8.58	8.64 ± 0.11	...
10.1116	0.709	...	-21.10	8.96	> 8.95	...
10.1213	0.815	20.63 ± 0.16	-21.18	8.86	8.90 ± 0.16	10.22 ± 0.31
10.1608	0.729	20.92 ± 0.22	-20.67	8.72	...	10.03 ± 0.28
10.1925	0.783	20.98 ± 0.16	-21.17	8.82	8.87 ± 0.06	9.87 ± 0.31
10.2183	0.910	20.69 ± 0.12	-22.14	8.92	8.95 ± 0.03	10.30 ± 0.20
10.2284	0.773	21.46 ± 0.25	-20.78	8.76	> 8.61	9.85 ± 0.34
10.2418	0.796	20.14 ± 0.07	-22.23	9.02	> 9.00	10.56 ± 0.14
10.2428	0.872	21.61 ± 0.29	-21.49	8.50	8.54 ± 0.07	9.89 ± 0.16
10.2519	0.718	22.00 ± 0.41	-20.07	8.90	...	9.67 ± 0.21
10.2548	0.770	20.24 ± 0.08	-21.32	8.78	< 8.83	10.56 ± 0.12
14.0072	0.621	21.30 ± 0.54	-20.05	8.58	8.61 ± 0.07	9.55 ± 0.41
14.0129	0.903	20.63 ± 0.29	-21.16	8.92	> 8.90	10.53 ± 0.29
14.0217	0.721	...	-21.14	8.70	8.73 ± 0.08	...
14.0272	0.670	19.12 ± 0.07	-22.16	9.10	9.08 ± 0.03	10.52 ± 0.31
14.0393	0.603	19.76 ± 0.07	-22.00	8.86	8.90 ± 0.06	10.22 ± 0.15
14.0497	0.800	20.59 ± 0.14	-21.45	8.76	8.82 ± 0.10	10.05 ± 0.40
14.0538	0.810	...	-21.42	8.76	8.79 ± 0.03	...
14.0605	0.837	...	-20.94	8.78	8.81 ± 0.05	...
14.0725	0.580	20.39 ± 0.23	-19.92	9.00	9.02 ± 0.03	10.13 ± 0.25
14.0779	0.580	...	-20.28	8.98	9.00 ± 0.05	...
14.0818	0.901	...	-22.54	8.86	8.89 ± 0.08	...
14.0848	0.664	26.07 ± 9.99	-20.37	8.68	8.73 ± 0.12	...
14.0972	0.677	20.34 ± 0.22	-21.56	8.64	8.69 ± 0.06	9.92 ± 0.36
14.0985	0.809	21.20 ± 0.25	-20.76	8.92	8.94 ± 0.05	9.97 ± 0.26
14.1087	0.659	21.20 ± 0.25	-20.63	8.70	8.72 ± 0.08	9.53 ± 0.35
14.1126	0.746	...	-20.71	8.30	8.53 ± 0.14	...
14.1189	0.753	21.04 ± 0.22	-20.86	8.88	> 8.81	9.84 ± 0.32
14.1190	0.754	...	-21.99	9.08	> 9.05	...
14.1258	0.647	21.51 ± 0.34	-20.31	8.82	8.87 ± 0.03	9.59 ± 0.28
14.1386	0.744	19.90 ± 0.08	-21.67	8.98	9.01 ± 0.04	10.21 ± 0.44
14.1466	0.674	23.40 ± 3.70	-20.36	8.30	8.57 ± 0.12	...

TABLE 3
– *Continued*

ID	z	K	$M_{B,AB}$[a]	$12+\log(\mathrm{O/H})$		$\log M_\star$
		(mag)	(mag)	LCS	This paper[b]	[$M_\odot$]
14.9705	0.609	. . .	−21.22	8.78	8.83 ± 0.10	. . .
22.0274	0.504	19.90 ± 0.10	−21.60	8.52	8.53 ± 0.11	9.88 ± 0.39
22.0322	0.915	21.12 ± 0.31	−21.80	8.30	8.35 ± 0.22	9.93 ± 0.39
22.0417	0.593	21.22 ± 0.34	−20.30	8.80	8.86 ± 0.08	9.73 ± 0.35
22.0429	0.624	20.49 ± 0.17	−20.48	8.76	8.80 ± 0.09	10.07 ± 0.20
22.0576	0.887	. . .	−21.24	8.70	8.72 ± 0.04	. . .
22.0599	0.886	. . .	−21.78	8.76	8.80 ± 0.04	. . .
22.0770	0.816	22.29 ± 0.90	−21.47	8.30	8.60 ± 0.12	. . .
22.0919	0.472	. . .	−20.22	8.30	8.41 ± 0.04	. . .
22.1119	0.514	. . .	−21.87	8.86	8.90 ± 0.08	. . .
22.1313	0.817	21.16 ± 0.32	−21.54	8.54	8.61 ± 0.14	9.92 ± 0.45
22.1350	0.510	21.50 ± 0.44	−19.88	8.80	8.84 ± 0.06	9.55 ± 0.40
22.1528	0.665	21.84 ± 0.60	−20.54	8.60	8.65 ± 0.06	9.39 ± 0.41

[a]As reported in LCS.
[b]Errors do not include systematic uncertainties.